JACS
JOURNAL OF THE AMERICAN CHEMICAL SOCIETY
pubs.acs.org/JACS
Article

Peroxide-Selective Reduction of O_2 at Redox-Inactive Rare-Earth(III) Triflates Generates an Ambiphilic Peroxide

Matthew J. Lueckheide, Mehmed Z. Ertem,* Michael A. Michon, Pawel Chmielniak, and Jerome R. Robinson*

Cite This: J. Am. Chem. Soc. 2022, 144, 17295−17306
Read Online
ACCESS | Metrics & More | Article Recommendations | Supporting Information

ABSTRACT: Metal peroxides are key species involved in a range of critical biological and synthetic processes. Rare-earth (group III and the lanthanides; Sc, Y, La−Lu) peroxides have been implicated as reactive intermediates in catalysis; however, reactivity studies of isolated, structurally characterized rare-earth peroxides have been limited. Herein, we report the peroxide-selective (93−99% O_2^{2-}) reduction of dioxygen (O_2) at redox-inactive rare-earth triflates in methanol using a mild metallocene reductant, decamethylferrocene (Fc*). The first molecular praseodymium peroxide ($[Pr^{III}_2(O_2^{2-})(18C6)_2(EG)_2][OTf]_4$; 18C6 = 18-crown-6, EG = ethylene glycol, $^-OTf = {}^-O_3SCF_3$; **2-Pr**) was isolated and characterized by single-crystal X-ray diffraction, Raman spectroscopy, and NMR spectroscopy. **2-Pr** displays high thermal stability (120 °C, 50 mTorr), is protonated by mild organic acids [pK_{a1}(MeOH) = 5.09 ± 0.23], and engages in electrophilic (e.g., oxygen atom transfer) and nucleophilic (e.g., phosphate-ester cleavage) reactivity. Our mechanistic studies reveal that the rate of oxygen reduction is dictated by metal-ion accessibility, rather than Lewis acidity, and suggest new opportunities for differentiated reactivity of redox-inactive metal ions by leveraging weak metal−ligand binding events preceding electron transfer.

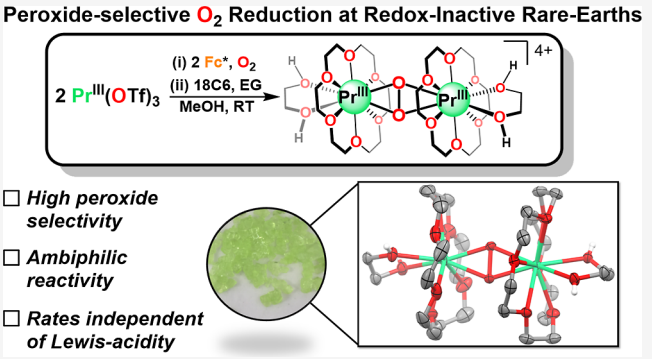

INTRODUCTION

Metal peroxides have been implicated as key species in a variety of biological and synthetic processes ranging from oxygen transport/storage,[1] energy storage,[2] medicine,[3] and catalysis (e.g., oxygen reduction,[4] water oxidation,[5] and organic oxidations[6]). Significant research efforts have been devoted to the isolation and characterization of molecular transition-metal peroxides, which in turn have uncovered novel structures featuring diverse binding modes, properties, and reactivity.[1b,7−14] These complexes can engage in mechanistically distinct oxidative reactivity,[15] where the peroxide fragment can display electrophilic,[7e,9e,f,11g,16] nucleophilic,[10j,17] or in rare instances, ambiphilic[11e,13d,16m,18] reactivity. In contrast, comparatively less is known regarding the chemistry of (alkyl-/hydro-)peroxides of the rare-earth elements (RE = Sc, Y, La−Lu). Such species have been proposed as reactive intermediates in a range of transformations, including the oxidative coupling of methane,[19] epoxidations,[20] and phosphate-ester cleavage,[21] yet reactivity studies of structurally characterized peroxides have been extremely limited.[22]

In terms of accessing metal peroxides, O_2 is an abundant and ideal oxidant; however, the limited kinetic reactivity of O_2 has generally restricted facile and high-yielding syntheses of O_2-derived metal peroxides to redox-active transition-metal ions and/or strongly reducing species. Consequentially, the synthesis of molecular RE^{III} peroxides derived from O_2 has effectively been limited to the use of strongly reducing RE^{II},[23] the N_2^{2-} ligand,[22a] or adventitious formation in low yields[24] and/or long time periods (3 weeks to 5 months)[25] from presumed ligand or solvent oxidation. Looking at the chemistry of other traditionally redox-inactive metal ions or main-group Lewis acids, several examples have been reported (Figure 1). Agapie and co-workers reported the direct synthesis of bis(borane) peroxides from O_2 using mild metallocene reductants (e.g., decamethylferrocene, Fc*, and ferrocene, Fc) with a strong main-group Lewis acid, $B(C_6F_5)_3$; however, control studies suggest that redox-active boron centers are operative (Figure 1A).[26] Greb and co-workers leveraged metal−ligand cooperativity in the synthesis of aluminum alkylperoxides, where inner-sphere reduction of O_2 was achieved with reducing equivalents sourced from the calix[4]-pyrrolato ligand after binding the Lewis acidic Al^{III} center (Figure 1B).[27] Szymczak and co-workers also leveraged metal−

Received: August 2, 2022
Published: September 9, 2022

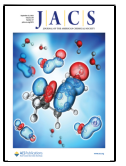

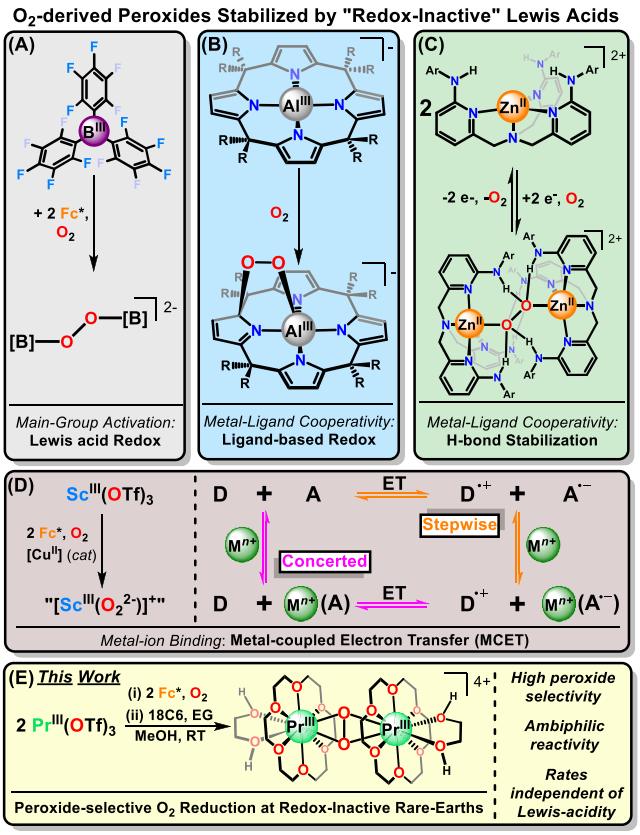

Figure 1. Examples of O_2-derived peroxides stabilized by "redox-inactive" Lewis acids. (A) Lewis acid redox, (B) ligand-based redox, (C) H-bond stabilization, (D) metal-coupled electron transfer (MCET), and (E) this work, O_2-derived rare-earth peroxides at redox-inactive rare earths.

ligand cooperativity in the synthesis of dizinc peroxides from O_2 and cobaltocene, where H-bonding interactions between the ligand secondary coordination-sphere and peroxide fragment were crucial in enabling the observed reactivity (Figure 1C).[28] Recently, Karlin, Fukuzumi, and co-workers accessed a scandium peroxide, "$[Sc^{III}(O_2^{2-})]^{+}$", through a copper-catalyzed reduction of O_2 in the presence of Fc* and $Sc^{III}(OTf)_3$; however, the structure and reactivity of the RE^{III} species remain unknown (Figure 1D).[29]

Fukuzumi and co-workers have established that the rates, selectivity, and thermodynamics of multi-e^- processes can be dramatically altered by redox-inactive metal ions through MCET.[30] In stepwise or concerted MCET processes (Figure 1D), reduction of an electron-acceptor (A) by a donor (D) can be accelerated by $\sim 10^8$ in the presence of strong redox-inactive metal ions (M^{n+}), where the rates of electron transfer track with Lewis acidity ($k_{ET}(M^{III}) \gg k_{ET}(M^{II}) \gg k_{ET}(M^{I})$).[31] This acceleration originates from the increased driving force for electron transfer due to stabilization of the reduced fragment upon metal-ion binding. Despite these observations, outside of the aforementioned Cu^{II}-catalyzed reduction of oxygen, such approaches have not been used to access O_2-derived metal peroxides. Herein, we report the peroxide-selective reduction of O_2 at redox-inactive $RE^{III}(OTf)_3$ using a mild metallocene reductant, Fc*. This leads to the isolation, characterization, and reactivity of the first Pr^{III} peroxide, where reactivity studies support ambiphilic character of a rare-earth peroxide fragment for the first time (Figure 1E). Our mechanistic studies support rate-limiting O_2 binding, which is sensitive to metal-ion size and speciation in solution rather than Lewis acidity. This unique dependence offers new opportunities for differentiated reactivity of redox-inactive metal ions by leveraging weak metal−ligand binding events preceding electron transfer.

RESULTS AND DISCUSSION

Synthesis and Characterization of 1-Pr and 2-Pr. Consistent with expectations based on formal reduction potentials, methanol solutions of rare-earth metal triflates [$RE^{III}(OTf)_3$; RE^{III} = Sc, Y, La, Pr, Nd, Sm, Gd, Dy, Er, Yb, and Lu] and decamethylferrocene (Fc*) were unreactive under rigorously anaerobic conditions [$E_{1/2}(RE^{III}(OTf)_3) \leq -1.15$ V versus NHE;[32] $E_{1/2}(Fc^*) = +0.1$ V vs NHE[33]]. Alternatively, addition of oxygen to these solutions led to a rapid color change from golden yellow to green, which corresponded to the formation of Fc^{*+} ($\lambda_{max} = 780$ nm, $\varepsilon = 500$ M^{-1} cm^{-1}) and reduction of oxygen. Spectrophotometric titrations revealed that two equivalents of Fc* were consumed for every equivalent of $RE^{III}(OTf)_3$ (Figure 2; RE^{III} = Pr), while

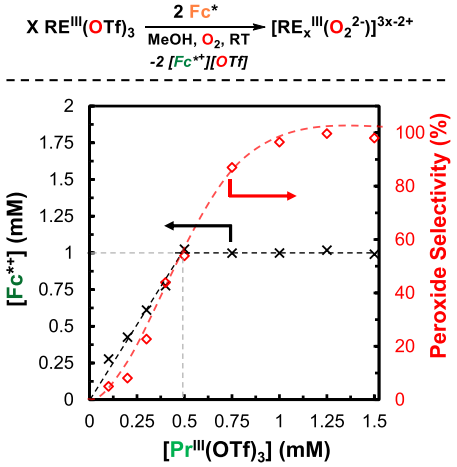

Figure 2. Spectrophotometric titrations following the reduction of O_2 (10 mM) by Fc* (1.0 mM) with $Pr^{III}(OTf)_3$ (0−1.5 mM) in MeOH at 298 K.

iodometry confirmed exclusive peroxide formation at ≥ 1:1 [Pr^{III}]:[Fc*] (peroxide selectivity = $[I_3^-]_{obs}/[O_2^{2-}]_{theo} \times 100\%$; $\lambda_{max}(I_3^-) = 358$ nm, $\varepsilon = 25$ mM^{-1} cm^{-1}; see the Supporting Information for additional details).

Isolation of a praseodymium peroxide with the empirical formula $[Pr^{III}_2(O_2^{2-})(OTf)_4(MeOH)_2]_n$ (**1-Pr**) was accomplished in 91% yield from the reaction of equimolar $Pr^{III}(OTf)_3$ and Fc* under an oxygen atmosphere (Figure 2). Confocal Raman microscopy unambiguously confirmed the presence of the peroxide fragment. **1-Pr** displayed a single isotopically sensitive vibration at 820 cm^{-1}, which falls within the range reported for other rare-earth peroxides.[22a,23a,24a,25a] A peroxide stretch was not observed for $^{18}O_2$-derived **1-Pr**, which we attribute to spectral overlap with a triflate C−F vibration[34] ($\nu_{C-F} = 770$ cm^{-1}; Theory: $\Delta^{18}O-^{18}O$(**1-Pr**) = 47 cm^{-1}, $\nu^{18}{}_{O-}{}^{18}{}_{O}$(**1-Pr**) = 773 cm^{-1}). Attempts to crystallize the alcohol solvate, **1-Pr**, only led to amorphous materials; however, introducing chelating O-donors, 18-crown-6 (18C6), and ethylene glycol (EG) furnished X-ray quality single crystals of the dimeric praseodymium peroxide,

https://doi.org/10.1021/jacs.2c08140
J. Am. Chem. Soc. 2022, 144, 17295−17306

$[Pr^{III}_2(O_2^{2-})$ $(18c6)_2(EG)_2][OTf]_4$ (**2-Pr**), in 72% yield from MeOH solutions layered with ^{i}PrOH (Figure 3).

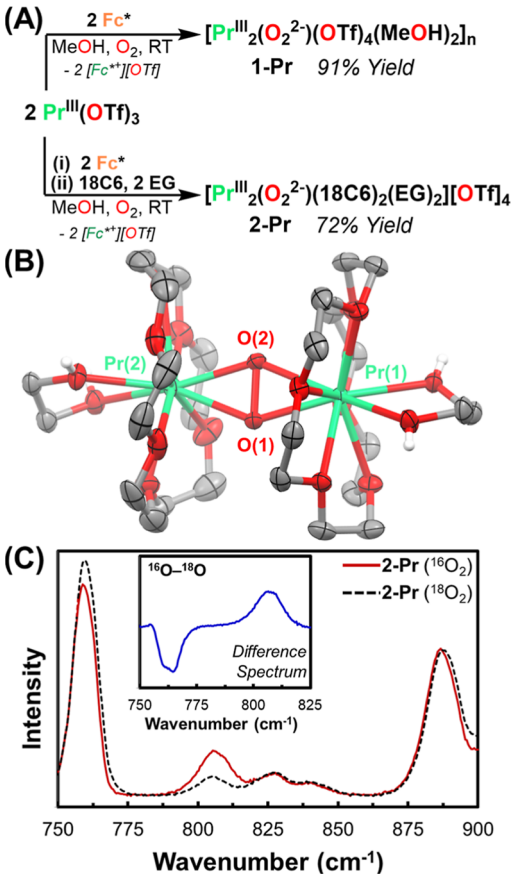

Figure 3. (A) Synthesis of **1-Pr** and **2-Pr**. (B) Thermal ellipsoid plot (50% probability) of **2-Pr**. Select bond metrics: Pr(1)−O(1) = 2.327(2) Å, Pr(1)−O(2) = 2.347(2) Å, Pr(2)−O(1) = 2.320(2) Å, Pr(2)−O(2) = 2.316(2) Å, O(1)−O(2) = 1.516(3) Å. (C) Raman spectrum (λ_{ex} = 532 nm) of $^{16}O_2$- and $^{18}O_2$-derived **2-Pr**. Inset: $^{16}O-^{18}O$ difference spectrum.

2-Pr is the first crystallographically characterized molecular praseodymium peroxide and features two, 10-coordinate Pr^{III} centers with an all *O*-donor coordination environment. The peroxide fragment is bound in a nearly symmetrical side-on fashion (μ:η^2:η^2), where the Pr−O distances [2.316(2)−2.347(2) Å] and O−O distances [1.516(3) Å] are comparable to those of other dimeric RE^{III} peroxides after accounting for differences in ionic radii.[22a,23a−c,25b−e] Direct observation of ν_{O-O} in **2-Pr** prepared from $^{16}O_2$ and $^{18}O_2$ was not possible due to overlap with ν_{C-O}(18C6) and ν_{C-F}(OTf) for ^{16}O- and ^{18}O-labeled **2-Pr** (Figure 3C), respectively; however, difference spectra revealed isotopically sensitive peaks consistent with a peroxide fragment and expectations based on an isolated harmonic oscillator model [$\Delta^{16}O-^{18}O$: Theory = 46 cm^{-1}, Expt = 43 cm^{-1}; $\nu^{16}{}_{O-}{}^{16}{}_{O}$(**2-Pr**) = 805 cm^{-1}, $\nu^{18}{}_{O-}{}^{18}{}_{O}$(**2-Pr**) = 762 cm^{-1}]. Multi-nuclear NMR studies confirmed that the solid-state structure of **2-Pr** was maintained in solution. The ^1H NMR spectrum of **2-Pr** collected in CD_3CN (Figure S14) displayed 6 paramagnetically shifted peaks over the range of +5 to −30 ppm corresponding to bound 18C6 and a single signal for free EG (displaced by CD_3CN). The ^{19}F NMR spectrum displayed a single broadened resonance at −71.78 ppm, which was consistent with labile triflate (Figure S15). **2-Pr** is non-hygroscopic, stable up to 120 °C at 50 mTorr in the solid state, and stable under N_2 or O_2 in refluxing MeOH or MeCN.

Reactivity Studies of 2-Pr. Despite proposals of rare-earth (hydro/alkyl) peroxides as reactive intermediates in the oxidative coupling of methane,[19] epoxidations,[20] and phosphate-ester cleavage,[21] reactivity studies of isolated species have been extremely limited. Evans reduced the dinuclear yttrium peroxide, $Y^{III}_2(\mu\text{-}O_2^{2-})[N(SiMe_3)_2]_4(THF)_2$, with KC_8 to form the corresponding bis-μ-oxo, $Y^{III}_2(\mu\text{-}O^{2-})_2[N(SiMe_3)_2]_4(THF)_2$.[22a] Kortz reported a hexacerium peroxide polyoxometalate, $[Ce^{IV}_6(\mu\text{-}O_2^{2-})_9(GeW_{10}O_{37})_3]^{24-}$, which promoted the stoichiometric and catalytic (H_2O_2) oxidation of methionine to the corresponding sulfoxide.[22b] Finally, Mashima reported a dinuclear cerium peroxide, $[Ce^{IV}_2(\mu\text{-}O_2^{2-})(L)_2(NO_3)_2]$ (L = $NH(CH_2CH_2N{=}CHC_6H_2$-3,5-$(^tBu)_2$-2-O)$_2$), which performed H-atom abstraction from TEMPOH to form the corresponding μ-oxo, $[Ce^{IV}_2(\mu\text{-}O^{2-})(L)_2(NO_3)_2]$.[22c,35] In contrast, isolated transition-metal peroxides display a diverse range of reactivity, including epoxidation,[6e,36] aldehyde deformylation,[37] hydrogen-atom transfer (HAT),[16p,38] oxygen-atom transfer (OAT)],[13d,39] and C-H activation.[16o,40] Given the paucity of reactivity studies of well-defined, soluble rare-earth peroxides, we investigated the ability of the peroxide fragment found in **2-Pr** to engage in acid−base, electrophilic, and nucleophilic reactions (Scheme 1).

Scheme 1. Reactivity of 2-Pr with Brønsted Acids, Nucleophiles, and Electrophiles

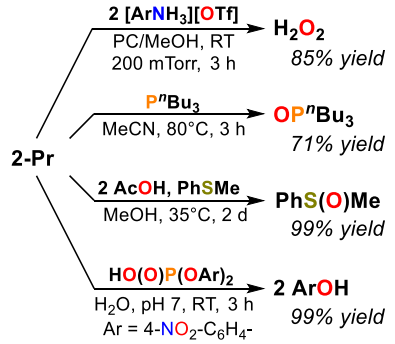

Spectrophotometric titration of **2-Pr** in MeOH using a weak organic acid, anilinium triflate ([$PhNH_3$][OTf], pK_a(MeOH) = 6.05),[41] was monitored by following the absorbance of the conjugate base ($PhNH_2$, λ_{max} = 285 nm, ε = 1867 M^{-1} cm^{-1}). Complete generation of H_2O_2 was achieved at [$PhNH_3$]-[OTf]/[**2-Pr**] of ∼60, and pK_{a1} (5.09 ± 0.23) was determined from early titration points following procedures adapted for monoprotic systems (Figure S73).[42] Given the absence of equivalence points and lack of suitable absorption features to distinguish Pr^{III} speciation, only rough estimates for pK_{a2} can be made (5.1 > pK_{a2} ≥ 4.5; see the Supporting Information for further discussion). Further confirmation of the observed acid−base reactivity was obtained from the recovery of H_2O_2 by vacuum transfer (85% yield, Scheme 1) following protonation of **2-Pr** by stoichiometric *p*-nitroanilinium triflate [pK_a(MeOH) = 1.55].[41]

Electrophilic reactivity of the peroxide fragment of **2-Pr** was established by evaluating its ability to perform OAT with organic nucleophiles (Scheme 1). Under rigorously anaerobic

https://doi.org/10.1021/jacs.2c08140
J. Am. Chem. Soc. 2022, 144, 17295−17306

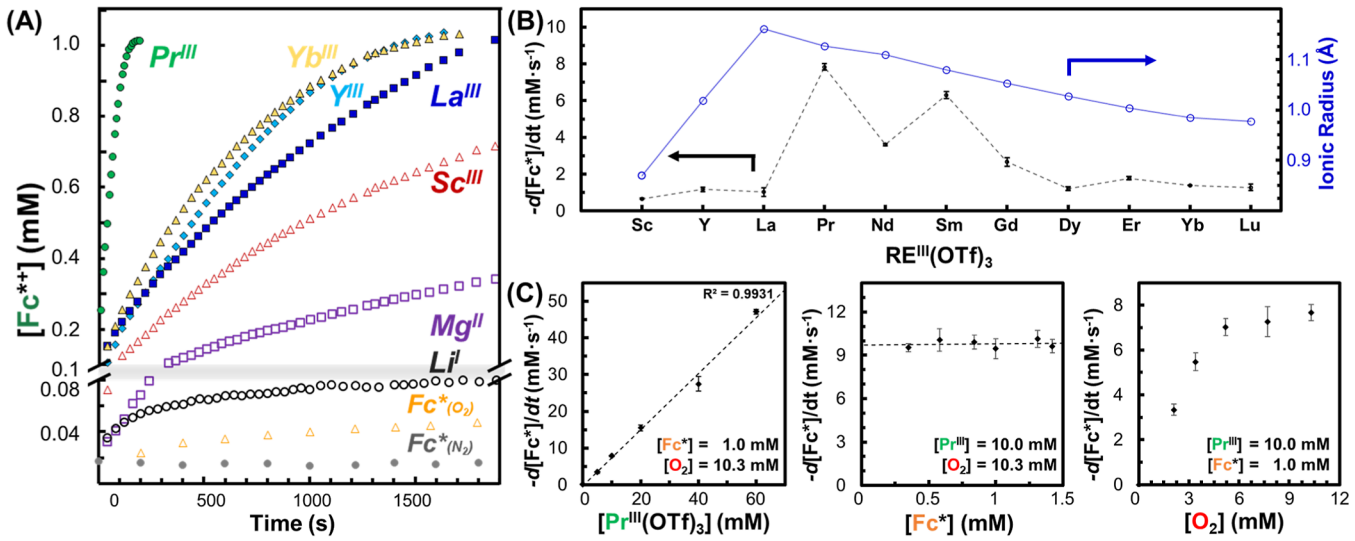

Figure 4. (A) Kinetic profiles for the reduction of O_2 (10.3 mM) by Fc* (1 mM) in the presence of $M^{n+}(OTf)_n$ (10 mM) in MeOH at 298 K. (B) Initial rates for the reduction of O_2 (10.3 mM) by Fc* (1 mM) in the presence of $M^{n+}(OTf)_n$ (10 mM) in MeOH at 298 K (*left*) and ionic radius (*right*). Error bars = 2σ. (C) Dependence of initial rate constants on $[Pr^{III}(OTf)_3]$, [Fc*], or $[O_2]$ (conditions in inset). Error bars = 2σ.

conditions, **2-Pr** performs OAT to P^nBu_3 to form OP^nBu_3 in 3 h at 80 °C in MeCN, while key control experiments confirm that **2-Pr** is stable in MeCN at 80 °C for days in the absence of substrate (Table S8, Entry 3). Complete consumption of **2-Pr** and P^nBu_3 was confirmed by iodometry and ^{31}P NMR, respectively, while OP^nBu_3 was quantified by ^{31}P NMR spectroscopy after removal of praseodymium by precipitation with oxalic acid and triethylamine (71% yield; Section S8, Figures S75 and S76). While **2-Pr** was unreactive with a weaker nucleophile, thioanisole (PhSMe), addition of stoichiometric acetic acid [pK_a(MeOH) = 9.63][41] led to quantitative formation of methylphenyl sulfoxide [PhS(O)Me] (Figures S77 and S78, Table S8). Although the pK_a of AcOH is ~5 units higher than that of $pK_{a,1}$ of **2-Pr**, reactivity from small amounts of a reactive rare-earth hydroperoxide cannot be rigorously excluded.

Chin reported that at pH 7 (N-(2-hydroxyethyl)piperazine-N′-ethanesulfonic acid, HEPES, buffer) in the presence of H_2O_2, $RE^{III}(ClO_4)_3$ accelerated phosphodiester cleavage (P−OR bonds) of bis(nitrophenyl) phosphate (BNPP) by ~10^8.[21b−d] Variable pH kinetic studies suggested that low concentrations (K_{eq} ~ 1.4×10^{-23} M) of soluble, dimeric RE^{III} bis(peroxide) species, $[RE^{III}_2(O_2^{2-})_2]^{2+}$, were the active species. Furthermore, the use of ^{18}O-labeled H_2O_2 implicated that a *nucleophilic* peroxide fragment was responsible for the rapid P−OR cleavage. Under identical conditions, electronic absorption spectroscopy revealed that **2-Pr**, $[Pr^{III}(18C6)(EG)_2][OTf]_3$ (**3-Pr**)/H_2O_2, and $Pr^{III}(OTf)_3/H_2O_2$ react with BNPP at comparable rates (within ~twofold, Figure S80) to release 2 equiv of *p*-nitrophenol (Scheme 1). This marks the first demonstration of nucleophilic reactivity from an isolated rare-earth peroxide (i.e., **2-Pr**) and supports ambiphilic character of the $RE^{III}_2(\mu{:}\eta^2{:}\eta^2{-}O_2^{2-})$ fragment.

Mechanism of O_2 Reduction. Mechanistic insights into the peroxide-selective reduction of oxygen was provided by initial-rate kinetic studies performed under flooding conditions and monitored by UV−visible spectroscopy (Fc^{*+}: λ_{max} = 780 nm; ε = 500 M^{-1} cm^{-1}; [Fc*] = 1 mM, $[O_2]_{sat}$ = 10.3 mM, $[M^{n+}(OTf)_n]$ = 10 mM; Figure 4A and S22-37). Full conversion and high peroxide selectivity were observed for all $RE^{III}(OTf)_3$ (93−99%; Table S3), while weaker mono- and divalent Lewis acids [e.g., $Li^I(OTf)$ and $Mg^{II}(OTf)_2$] only reached partial conversion and formed trace amounts of peroxide (Figures S28 and S29). Unlike other electron-transfer reactions that are accelerated in the presence of redox-inactive metal ions,[30] the rate of Fc^{*+} formation did not follow expectations based on Lewis acidity (Sc^{III} > Yb^{III} > Y^{III} > Pr^{III} ~ La^{III}). Instead, the most Lewis acidic cation, Sc^{III}, was >10-fold *slower* than the fastest RE^{III} and Pr^{III}, and rates varied significantly depending on the RE^{III} ionic radius (Figure 4B).

Control experiments evaluating the potential involvement of trace-metal impurities were performed with $RE^{III}(OTf)_3$ obtained from multiple sources and varying purity levels (98, 99.9, or 99.995%; all samples were ≥99.9% purity rare-earth oxide, REO; Figures S23 and S26). Comparable rates and selectivities were observed, making the involvement of trace-metal impurities unlikely. Further control experiments revealed that only small amounts of Fc^{*+} (~4%) and no peroxide formed under identical conditions in the absence of $M^{n+}(OTf)_n$ (Figures 4A and S38). Although disfavored in alcohols,[43] auto-oxidation of ferrocene derivatives in the presence of Brønsted acids and/or bases can occur through a radical-chain process.[43,44] Addition of a known inhibitor of radical-chain processes involving ferrocene derivatives,[43c] butylated hydroxytoluene (BHT; [BHT] = 10 $[Pr^{III}(OTf)_3]$), had no impact on the rate of Fc^{*+} formation and discounted a radical-chain mechanism (Figure S68).

Rate orders for $Pr^{III}(OTf)_3$, Fc*, and O_2 were established while maintaining at least a 10-fold excess of $Pr^{III}(OTf)_3$ and O_2 relative to Fc*. Under these conditions, initial rates displayed a first-order dependence on $[Pr^{III}(OTf)_3]$, a saturation dependence on $[O_2]$, and *a zero-order dependence on [Fc*]* (Figure 4C, eq 1, Figures S40−S53).

$$\text{rate} = k_{obs}[Pr^{III}]^1[O_2]^x; \qquad x = 0 - 1 \tag{1}$$

The zero-order dependence on the reductant was further confirmed by using octamethylferrocene (Me_8Fc) in place of Fc*, where the reduced driving force for electron transfer (~190 mV) led to only a ~twofold decrease in the initial rate (Fc* = 9.41 ± 0.53 × 10^{-3} mM/s; Me_8Fc = 5.4 ± 0.34 × 10^{-3}

https://doi.org/10.1021/jacs.2c08140
J. Am. Chem. Soc. 2022, 144, 17295−17306

mM/s). This contrasts with the expectations for stepwise or concerted MCET (first-order dependence on reductant)[30a,b] and suggests an alternative mechanism in which electron transfer is not rate determining.

Solvation and speciation are well known to play a key role in the structure and reactivity of labile rare-earth salts in organic solvent,[45] including $RE^{III}(OTf)_3$,[46] and motivated further experimental studies to establish the relevant structures of $RE^{III}(OTf)_3$ in MeOH. Conductivity measurements of anhydrous MeOH solutions of $RE^{III}(OTf)_3$ ($[RE^{III}]$ = 1 and 10 mM) fall within the range of 1:1 and 2:1 electrolytes in MeOH (Tables S10-11; RE^{III}:Sc, Y, La, and Pr)[47] and align with speciation proposed by Bünzli[48] for $La^{III}(OTf)_3$ or by Peters[47b] for $Dy^{III}(OTf)_3$ using ^{139}La NMR and quantitative vibrational spectroscopy or ^{17}O and ^{19}F NMR spectroscopy, respectively (i.e., $[Ln(OTf)_x(MeOH)_n][OTf]_{3-x}$; $x = 1-2$, $n = 5-7$). Addition of 100 mM $[NBu_4][OTf]$ had no effect on initial rates of Fc^{*+} formation and disfavors rate-determining triflate exchange (Figure S69).

On the basis of our experimental results, we propose a mechanism that is consistent with the observed kinetic behavior and rate orders (Scheme 2). The first-order dependence on $[Pr^{III}]$ and saturation dependence on $[O_2]$ support an equilibrium involving a solvated $Pr^{III}(OTf)_3$ species, $[Pr^{III}(OTf)_x(MeOH)_n]^{3-x+}$ ($[Pr^{III}]$), followed by rapid, irreversible O_2 binding to the activated Pr^{III} species, $[Pr^{III}(OTf)_x(MeOH)_n]^{3-x+}$* ($[Pr^{III}]$*). The O_2 adduct, $[Pr^{III}(O_2)(OTf)_x(MeOH)_n]^{3-x+}$ ($[Pr^{III}(O_2)]$), would undergo rapid, sequential reduction by Fc* (i.e., MCET), which, in the presence of an additional equivalent of $Pr^{III}(OTf)_3$, would generate **1-Pr**. Application of the steady-state approximation to $[Pr^{III}]$* leads to the kinetic expression in eq 2. Saturation behavior in $[O_2]$ would be achieved when $k_2[O_2] \gg k_{-1}$ and would lead to the simplified observed rate law in eq 1.

$$-2\frac{d[Fc^{*+}]}{dt} = -\frac{d[Pr^{III}(O_2)]}{dt} = \frac{k_1 k_2 [Pr^{III}][O_2]}{k_{-1} + k_2[O_2]} \quad (2)$$

Further support for the proposed mechanism came from kinetic modeling and activation parameters. Preliminary modeling of the initial-rate kinetic data using COPASI[49] provided estimates of k_{-1} (1.43 ± 0.78 s^{-1}) and k_2 (153 ± 80 $M^{-1}\cdot s^{-1}$), along with the experimentally measured value, k_1 (7.67 ± 0.36 × 10^{-4} s^{-1}). Simulated time courses with these values produced rate orders that were in excellent agreement with the experiment (Figure S82). Furthermore, experimentally determined activation parameters obtained from Eyring analysis of variable temperature kinetic studies (243−298 K) revealed a small enthalpic barrier and significant ordering for $Pr^{III}(OTf)_3$ ($\Delta H^{\ddagger}$ = 4.1 kcal/mol and $\Delta S^{\ddagger}$ = −44.3 cal/mol·K; $\Delta G^{\ddagger}_{298}$ = 17.3 kcal/mol). Evaluation of other $RE^{III}(OTf)_3$ (RE^{III} = Sc, Y, La) revealed comparable activation parameters and supports a conserved mechanism across the series (Figure 5; $\Delta H^{\ddagger}$: 4.1 to 7.7 kcal/mol; $\Delta S^{\ddagger}$: −38.4 to −44.3 cal/mol·K; $\Delta G^{\ddagger}_{298}$: 17.3 to 19.1 kcal/mol). The large, negative values for $\Delta S^{\ddagger}$ are in line with solvation playing a prominent role in the rate-determining step.

Complementary computational modeling studies were also carried out at the M06-L level of theory[50] in conjunction with SMD continuum solvation model[51] for methanol as the solvent (for the computational methods, see the Supporting Information). Given the active role of solvent dynamics and the possible errors that could originate from the computation of entropy changes for association/dissociation events of solvent molecules and O_2, we limit the mechanistic discussion to computed enthalpy changes (ΔH; see Tables S17−S25 for the complete list of computed ΔH and ΔG values). The enthalpy changes for MeOH exchange (ΔH_1), O_2 binding (ΔH_2), sequential reductions by Fc* (ΔH_3 & ΔH_4), and formation of dinuclear peroxides (ΔH_5) for representative $RE^{III}(OTf)_3$ (RE^{III} = Sc, Y, La, and Pr) were calculated starting from all plausible methanol-solvated 1:1 and 1:2 electrolytes (Tables S17−S25). MeOH dissociation from coordinatively

Scheme 2. Proposed Mechanism

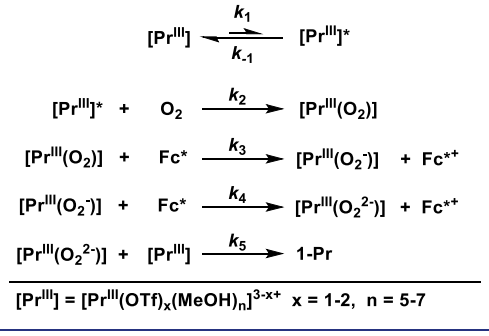

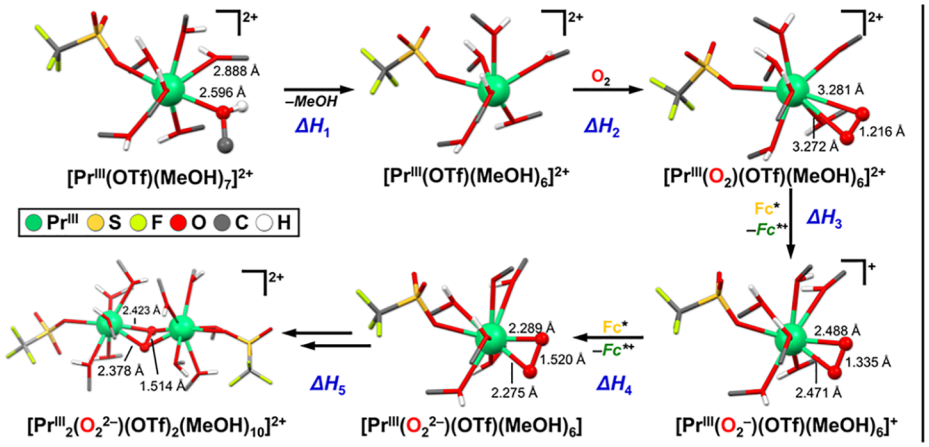

[RE^III]	[Sc^III]	[Y^III]	[La^III]	[Pr^III]
ΔH_1[a]	12.0	4.3	4.6	5.0
ΔH_2[a]	-1.5	-1.0	-3.2	-2.4
ΔH_3[a]	-33.3	-16.4	-8.9	-12.4
ΔH_4[a]	-15.2	-0.2	5.6	2.2
ΔH_5[a]	-24.2	-8.4	-15.8	-17.6
$\Delta G^{\ddagger}$[a]	19.1	18.6	18.8	17.3
$\Delta H^{\ddagger}$[a]	7.7	6.5	6.8	4.1
$\Delta S^{\ddagger}$[b]	-38.4	-40.8	-40.3	-44.3

a - kcal/mol *b* - cal/mol·K

Figure 5. (Left) DFT-calculated structures for the reduction of O_2 by $Pr^{III}(OTf)_3$ in MeOH. (Right) *Top*: Enthalpy changes for the calculated structures of $RE^{III}(OTf)_3$ (RE^{III} = Sc^{III}, Y^{III}, La^{III}, Pr^{III}). *Bottom*: Experimental activation parameters obtained from Eyring analysis.

https://doi.org/10.1021/jacs.2c08140
J. Am. Chem. Soc. 2022, 144, 17295−17306

saturated species was endothermic for all RE^{III} (ΔH_1: +4.3 to +12.0 kcal/mol), while coordination of the weak neutral donor, O_2, was modestly exothermic for all RE^{III} (ΔH_2: −1.0 to −3.2 kcal/mol). Single-electron reduction of the RE^{III} oxygen adduct to form the RE^{III} superoxide was exothermic and strongly correlated with Lewis acidity (ΔH_3: −8.9 to −33.3 kcal/mol). The trend in ΔH_3 follows expectations for concerted MCET[31a] and indicates a strong driving force for oxygen reduction at $RE^{III}(OTf)_3$. The RE^{III} superoxide can be further reduced by Fc* to a terminal RE^{III} peroxide (ΔH_4: −15.2 to +5.6 kcal/mol), which can readily form a stable dinuclear peroxide with a second equivalent of $RE^{III}(OTf)_3$ (ΔH_5 = −24.2 to −8.4 kcal/mol).

Taken together, our mechanistic studies revealed that the formation of RE^{III} peroxides at redox-inactive $RE^{III}(OTf)_3$, O_2, and Fc* *does not* proceed through rate-limiting MCET. Instead of rates being driven by differences in Lewis acidity,[30b,31a] the rate of Fc^{*+} formation is controlled by differences in RE^{III} solvation and their ability to interact with the weak neutral donor, O_2. We propose that the change in rate-determining steps originates from the relative interaction strength between the Lewis acid and O_2 fragment. In most examples of rate-determining MCET involving O_2, transition metals rapidly bind O_2 and induce partial or full charge transfer.[29,30] The enhanced charge density would be expected to increase the affinity of the O_2 fragment for hard, ionic Lewis acids over that of neutral Lewis bases (e.g., solvent). While the reduction of O_2 by Fc* in the presence of $RE^{III}(OTf)_3$ is slower than when redox-active transition metals are present, this opens an alternative mechanistic pathway with distinct periodic trends in reactivity. Although size- and solvation-dependent trends are pervasive in the chemistry of the lanthanide series (e.g., "gadolinium break"[52] and tetrad effects[53]), the discovery of systems with non-monotonic trends in thermodynamic and/or kinetic behavior across the lanthanide series remains rare.[54] Our results suggest that differences in solvation of even simple and highly labile RE^{III} salts can lead to significant kinetic reactivity differences of chemically similar, neighboring lanthanides and might be further amplified through appropriate ligand design.

While our computational modeling studies capture the key role that MCET plays in the driving force for peroxide formation in post-rate-determining steps, further efforts are needed to capture properties and reactivity of these labile and heavily solvated species. Our exhaustive characterization of RE^{III} solvent speciation leading to O_2 binding provides initial snapshots but is limited to the first solvation shell (i.e., primary coordination sphere). Elegant modeling studies by Ramírez-Solís have demonstrated that the dynamic microsolvation environment of labile RE salts (e.g., $Sm^{II}X_2$ (X = Br, I) and $Sm^{III}I_3$) experimentally explored by Flowers can be captured through dynamic quantum mechanical approaches,[55] and similar approaches may be necessary to resolve the observed kinetic behavior in these and similar systems.

CONCLUSIONS

We have discovered a peroxide-selective reduction of oxygen mediated by redox-inactive RE^{III} in the presence of a mild reducing agent, Fc*. This allows for a simple and high-yielding synthesis of the first structurally characterized praseodymium peroxide, **2-Pr**. The dinuclear peroxide displays good thermal stability, is readily protonated by mild organic acids, and engages in electrophilic and nucleophilic reactivity. This is a rare demonstration of ambiphilic metal peroxide reactivity and is the first example for a rare-earth metal. Our mechanistic studies revealed that the rate of oxygen reduction does not proceed through rate-limiting MCET, as rates are independent of Lewis acid strength and exhibit a zero-order dependence on [Fc*]. Instead, the observed rates effectively follow RE^{III} accessibility to O_2, which is impacted by metal-ion size and solution speciation. This unique dependence offers new opportunities for differentiated reactivity of redox-inactive RE^{III} by leveraging weak metal−ligand binding events preceding electron transfer. Studies leveraging these weak interactions in stoichiometric and catalytic small-molecule transformations are ongoing.

ASSOCIATED CONTENT

Supporting Information

The Supporting Information is available free of charge at https://pubs.acs.org/doi/10.1021/jacs.2c08140.

Coordinates of DFT-optimized structures for Sc triflate species and O_2-bound species in MeOH (XYZ)

Coordinates of DFT-optimized structures for Y triflate species and O_2-bound species in MeOH (XYZ)

Coordinates of DFT-optimized structures for La triflate species and O_2-bound species in MeOH (XYZ)

Coordinates of DFT-optimized structures for Pr triflate species and O_2-bound species in MeOH (XYZ)

Detailed materials and methods including synthetic details, spectrophotometric titrations, reactivity studies, single-crystal X-ray diffraction experiments, Raman measurements, NMR spectra, UV−Vis kinetic data, and computational methods (PDF)

Accession Codes

CCDC 2189160−2189161 contain the supplementary crystallographic data for this paper. These data can be obtained free of charge via www.ccdc.cam.ac.uk/data_request/cif, or by emailing data_request@ccdc.cam.ac.uk, or by contacting The Cambridge Crystallographic Data Centre, 12 Union Road, Cambridge CB2 1EZ, UK; fax: +44 1223 336033.

AUTHOR INFORMATION

Corresponding Authors

Mehmed Z. Ertem − *Chemistry Division, Energy & Photon Sciences, Brookhaven National Laboratory, Upton, New York 11973, United States;* orcid.org/0000-0003-1994-9024; Email: mzertem@bnl.gov

Jerome R. Robinson − *Department of Chemistry, Brown University, Providence, Rhode Island 02912, United States;* orcid.org/0000-0002-9111-3822; Email: jerome_robinson@brown.edu

Authors

Matthew J. Lueckheide − *Department of Chemistry, Brown University, Providence, Rhode Island 02912, United States;* orcid.org/0000-0003-3590-6112

Michael A. Michon − *Department of Chemistry, Brown University, Providence, Rhode Island 02912, United States*

Pawel Chmielniak − *Department of Chemistry, Brown University, Providence, Rhode Island 02912, United States*

Complete contact information is available at: https://pubs.acs.org/10.1021/jacs.2c08140

Notes

The authors declare no competing financial interest.

■ ACKNOWLEDGMENTS

The work at Brown University (J.R.R., M.J.L.) was financially supported by the National Science Foundation (CHE-1900248) and Brown University (start-up funds). The work at Brookhaven National Laboratory (M.Z.E) was carried out under contract DE-SC0012704 with the U.S. Department of Energy, Office of Science, Office of Basic Energy Sciences, and utilized computational resources at the Center for Functional Nanomaterials, which is a U.S. Department of Energy Office of Science Facility, and the Scientific Data and Computing Center, a component of the Computational Science Initiative, at Brookhaven National Laboratory under contract no. DE-SC0012704. J.R.R. and M.J.L. thank Prof. Eunsuk Kim, Dr. Natasha P. Vargo, Alex M. Brown, and Peter Saghy for helpful discussions and Prof. Christoph Rose-Petruck for the use of his Raman spectrometer.

■ REFERENCES

(1) (a) Bertini, I.; Bertini, G.; Gray, H. B.; Gray, P. H.; Valentine, J. S.; Stiefel, E. I.; Stiefel, P. E.*Biological Inorganic Chemistry: Structure and Reactivity*; University Science Books, 2007, pp 319−442. (b) Jasniewski, A. J.; Que, L. Dioxygen Activation by Nonheme Diiron Enzymes: Diverse Dioxygen Adducts, High-Valent Intermediates, and Related Model Complexes. *Chem. Rev.* **2018**, *118*, 2554−2592. (c) Solomon, E. I.; Heppner, D. E.; Johnston, E. M.; Ginsbach, J. W.; Cirera, J.; Qayyum, M.; Kieber-Emmons, M. T.; Kjaergaard, C. H.; Hadt, R. G.; Tian, L. Copper active sites in biology. *Chem. Rev.* **2014**, *114*, 3659−3853. (d) Stenkamp, R. E. Dioxygen and Hemerythrin. *Chem. Rev.* **1994**, *94*, 715−726. (e) Vaska, L. Dioxygen-metal complexes: toward a unified view. *Acc. Chem. Res.* **1976**, *9*, 175−183. (f) Vaska, L. Oxygen-Carrying Properties of a Simple Synthetic System. *Science* **1963**, *140*, 809−810. (g) Tokuichi, T. Nebenvalenzringverbindungen. IV. Über einige innerkomplexe Kobaltsalze der Oxyaldimine. *Bull. Chem. Soc. Jpn.* **1938**, *13*, 252−260.

(2) (a) Wang, H.-F.; Xu, Q. Materials Design for Rechargeable Metal-Air Batteries. *Matter* **2019**, *1*, 565−595. (b) Li, C.-S.; Sun, Y.; Gebert, F.; Chou, S.-L. Current Progress on Rechargeable Magnesium-Air Battery. *Adv. Energy Mater.* **2017**, *7*, 1700869. (c) Sun, W.; Wang, F.; Zhang, B.; Zhang, M.; Küpers, V.; Ji, X.; Theile, C.; Bieker, P.; Xu, K.; Wang, C.; Winter, M. A rechargeable zinc-air battery based on zinc peroxide chemistry. *Science* **2021**, *371*, 46−51. (d) Peng, Z.; Freunberger, S. A.; Chen, Y.; Bruce, P. G. A Reversible and Higher-Rate Li-O 2 Battery. *Science* **2012**, *337*, 563−566.

(3) (a) He, J.; Fu, L. H.; Qi, C.; Lin, J.; Huang, P. Metal peroxides for cancer treatment. *Bioact. Mater* **2021**, *6*, 2698−2710. (b) Hu, H.; Yu, L.; Qian, X.; Chen, Y.; Chen, B.; Li, Y. Chemoreactive Nanotherapeutics by Metal Peroxide Based Nanomedicine. *Adv. Sci.* **2021**, *8*, 2000494.

(4) (a) Machan, C. W. Advances in the Molecular Catalysis of Dioxygen Reduction. *ACS Catal.* **2020**, *10*, 2640−2655. (b) Pegis, M. L.; Wise, C. F.; Martin, D. J.; Mayer, J. M. Oxygen Reduction by Homogeneous Molecular Catalysts and Electrocatalysts. *Chem. Rev.* **2018**, *118*, 2340−2391. (c) Zhang, W.; Lai, W.; Cao, R. Energy-Related Small Molecule Activation Reactions: Oxygen Reduction and Hydrogen and Oxygen Evolution Reactions Catalyzed by Porphyrin- and Corrole-Based Systems. *Chem. Rev.* **2017**, *117*, 3717−3797.

(5) (a) Lubitz, W.; Chrysina, M.; Cox, N. Water oxidation in photosystem II. *Photosynth* **2019**, *142*, 105−125. (b) Hunter, B. M.; Gray, H. B.; Müller, A. M. Earth-Abundant Heterogeneous Water Oxidation Catalysts. *Chem. Rev.* **2016**, *116*, 14120−14136. (c) Blakemore, J. D.; Crabtree, R. H.; Brudvig, G. W. Molecular Catalysts for Water Oxidation. *Chem. Rev.* **2015**, *115*, 12974−13005. (d) Cox, N.; Pantazis, D. A.; Neese, F.; Lubitz, W. Biological Water Oxidation. *Acc. Chem. Res.* **2013**, *46*, 1588−1596. (e) Gilbert, J. A.; Eggleston, D. S.; Murphy, W. R.; Geselowitz, D. A.; Gersten, S. W.; Hodgson, D. J.; Meyer, T. J. Structure and redox properties of the water-oxidation catalyst [(bpy)2(OH2)RuORu(OH2)(bpy)2]4+. *J. Am. Chem. Soc.* **1985**, *107*, 3855−3864.

(6) (a) Liang, Y.; Wei, J.; Qiu, X.; Jiao, N. Homogeneous Oxygenase Catalysis. *Chem. Rev.* **2018**, *118*, 4912−4945. (b) Grant, J. T.; Venegas, J. M.; McDermott, W. P.; Hermans, I. Aerobic Oxidations of Light Alkanes over Solid Metal Oxide Catalysts. *Chem. Rev.* **2018**, *118*, 2769−2815. (c) Wang, D.; Weinstein, A. B.; White, P. B.; Stahl, S. S. Ligand-Promoted Palladium-Catalyzed Aerobic Oxidation Reactions. *Chem. Rev.* **2018**, *118*, 2636−2679. (d) Huang, X.; Groves, J. T. Oxygen Activation and Radical Transformations in Heme Proteins and Metalloporphyrins. *Chem. Rev.* **2018**, *118*, 2491−2553. (e) Bryliakov, K. P. Catalytic Asymmetric Oxygenations with the Environmentally Benign Oxidants H2O2 and O2. *Chem. Rev.* **2017**, *117*, 11406−11459. (f) Allen, S. E.; Walvoord, R. R.; Padilla-Salinas, R.; Kozlowski, M. C. Aerobic Copper-Catalyzed Organic Reactions. *Chem. Rev.* **2013**, *113*, 6234−6458. (g) Adam, W.; Malisch, W.; Roschmann, K. J.; Saha-Möller, C. R.; Schenk, W. A. Catalytic oxidations by peroxy, peroxo and oxo metal complexes: an interdisciplinary account with a personal view. *J. Organomet. Chem.* **2002**, *661*, 3−16. (h) Kühn, F. E.; Herrmann, W. A.Rhenium-Oxo and Rhenium-Peroxo Complexes in Catalytic Oxidations. In *Metal-Oxo and Metal-Peroxo Species in Catalytic Oxidations*; Meunier, B., Ed.; Springer Berlin Heidelberg: Berlin, Heidelberg, 2000; pp 213−236. (i) Katsuki, T.; Sharpless, K. B. The first practical method for asymmetric epoxidation. *J. Am. Chem. Soc.* **1980**, *102*, 5974−5976.

(7) **Group IV:** (a) Oyeka, E. E.; Oka, D.; Kwon, E.; Fukumura, T. Synthesis of Stoichiometric SrTiO3 and Its Carrier Doping from Air-Stable Bimetallic Complexes. *Inorg. Chem.* **2021**, *60*, 1277−1283. (b) Zhang, H.; Hatzis, G. P.; Moore, C. E.; Dickie, D. A.; Bezpalko, M. W.; Foxman, B. M.; Thomas, C. M. O2 Activation by a Heterobimetallic Zr/Co Complex. *J. Am. Chem. Soc.* **2019**, *141*, 9516−9520. (c) Stauber, J. M.; Cummins, C. C. Terminal Titanyl Complexes of Tri- and Tetrametaphosphate: Synthesis, Structures, and Reactivity with Hydrogen Peroxide. *Inorg. Chem.* **2017**, *56*, 3022−3029. (d) Berkessel, A.; Günther, T.; Wang, Q.; Neudörfl, J.-M. Titanium Salalen Catalysts Based oncis-1,2-Diaminocyclohexane: Enantioselective Epoxidation of Terminal Non-Conjugated Olefins with H2O2. *Angew. Chem., Int. Ed.* **2013**, *52*, 8467−8471. (e) Kondo, S.; Saruhashi, K.; Seki, K.; Matsubara, K.; Miyaji, K.; Kubo, T.; Matsumoto, K.; Katsuki, T. A μ-Oxo-μ-η2:η2-Peroxo Titanium Complex as a Reservoir of Active Species in Asymmetric Epoxidation Using Hydrogen Peroxide. *Angew. Chem., Int. Ed.* **2008**, *47*, 10195−10198. (f) Bassil, B. S.; Mal, S. S.; Dickman, M. H.; Kortz, U.; Oelrich, H.; Walder, L. 6-Peroxo-6-Zirconium Crown and Its Hafnium Analogue Embedded in a Triangular Polyanion: [M6(O2)6(OH)6-(γ-SiW10O36)3]18− (M = Zr, Hf). *J. Am. Chem. Soc.* **2008**, *130*, 6696−6697. (g) Stanciu, C.; Jones, M. E.; Fanwick, P. E.; Abu-Omar, M. M. Multi-electron Activation of Dioxygen on Zirconium(IV) to Give an Unprecedented Bisperoxo Complex. *J. Am. Chem. Soc.* **2007**, *129*, 12400−12401.

(8) **Group V:** (a) Conte, V.; Floris, B. Vanadium and molybdenum peroxides: synthesis and catalytic activity in oxidation reactions. *Dalton Trans.* **2011**, *40*, 1419−1436. (b) Bayot, D.; Devillers, M. Peroxo complexes of niobium(V) and tantalum(V). *Coord. Chem. Rev.* **2006**, *250*, 2610−2626. (c) Butler, A.; Clague, M. J.; Meister, G. E. Vanadium Peroxide Complexes. *Chem. Rev.* **1994**, *94*, 625−638. (d) Cozzolino, A. F.; Tofan, D.; Cummins, C. C.; Temprado, M.; Palluccio, T. D.; Rybak-Akimova, E. V.; Majumdar, S.; Cai, X.; Captain, B.; Hoff, C. D. Two-Step Binding of O2 to a Vanadium(III) Trisanilide Complex To Form a Non-Vanadyl Vanadium(V) Peroxo Complex. *J. Am. Chem. Soc.* **2012**, *134*, 18249−18252. (e) Van Asselt, A.; Trimmer, M. S.; Henling, L. M.; Bercaw, J. E. Dioxygen-derived peroxo-alkyl complexes of permethyltantalocene. Structural characterization of (.eta.5-C5Me5)2Ta(.eta.2-O2)(CH2C6H5) and acid-

https://doi.org/10.1021/jacs.2c08140
J. Am. Chem. Soc. 2022, 144, 17295−17306

catalyzed rearrangement to oxo-alkoxide derivatives. *J. Am. Chem. Soc.* **1988**, *110*, 8254−8255.

(9) **Group VI:** (a) Ramos, M. L.; Justino, L. L. G.; Burrows, H. D. Structural considerations and reactivity of peroxocomplexes of V(v), Mo(vi) and W(vi). *Dalton Trans.* **2011**, *40*, 4374−4383. (b) Dickman, M. H.; Pope, M. T. Peroxo and Superoxo Complexes of Chromium, Molybdenum, and Tungsten. *Chem. Rev.* **1994**, *94*, 569−584. (c) Wind, M.-L.; Hoof, S.; Braun-Cula, B.; Herwig, C.; Limberg, C. Switching from a Chromium(IV) Peroxide to a Chromium(III) Superoxide upon Coordination of a Donor in the trans Position. *J. Am. Chem. Soc.* **2019**, *141*, 14068−14072. (d) Yokoyama, A.; Han, J. E.; Cho, J.; Kubo, M.; Ogura, T.; Siegler, M. A.; Karlin, K. D.; Nam, W. Chromium(IV)-Peroxo Complex Formation and Its Nitric Oxide Dioxygenase Reactivity. *J. Am. Chem. Soc.* **2012**, *134*, 15269−15272. (e) Ishimoto, R.; Kamata, K.; Mizuno, N. A Highly Active Protonated Tetranuclear Peroxotungstate for Oxidation with Hydrogen Peroxide. *Angew. Chem., Int. Ed.* **2012**, *51*, 4662−4665. (f) Kamata, K.; Hirano, T.; Kuzuya, S.; Mizuno, N. Hydrogen-Bond-Assisted Epoxidation of Homoallylic and Allylic Alcohols with Hydrogen Peroxide Catalyzed by Selenium-Containing Dinuclear Peroxotungstate. *J. Am. Chem. Soc.* **2009**, *131*, 6997−7004. (g) Kamata, K.; Kuzuya, S.; Uehara, K.; Yamaguchi, S.; Mizuno, N. μ-η1:η1-Peroxo-Bridged Dinuclear Peroxotungstate Catalytically Active for Epoxidation of Olefins. *Inorg. Chem.* **2007**, *46*, 3768−3774.

(10) **Group VII:** (a) Kovacs, J. A. Tuning the Relative Stability and Reactivity of Manganese Dioxygen and Peroxo Intermediates via Systematic Ligand Modification. *Acc. Chem. Res.* **2015**, *48*, 2744−2753. (b) Leto, D. F.; Jackson, T. A. Peroxomanganese complexes as an aid to understanding redox-active manganese enzymes. *J. Biol. Inorg Chem.* **2014**, *19*, 1−15. (c) Pecoraro, V. L.; Baldwin, M. J.; Gelasco, A. Interaction of Manganese with Dioxygen and Its Reduced Derivatives. *Chem. Rev.* **1994**, *94*, 807−826. (d) Herrmann, W. A.; Fischer, R. W.; Scherer, W.; Rauch, M. U. Methyltrioxorhenium(VII) as Catalyst for Epoxidations: Structure of the Active Species and Mechanism of Catalysis. *Angew. Chem., Int. Ed.* **1993**, *32*, 1157−1160. (e) Yan Poon, P. C.; Dedushko, M. A.; Sun, X.; Yang, G.; Toledo, S.; Hayes, E. C.; Johansen, A.; Piquette, M. C.; Rees, J. A.; Stoll, S.; Rybak-Akimova, E.; Kovacs, J. A. How Metal Ion Lewis Acidity and Steric Properties Influence the Barrier to Dioxygen Binding, Peroxo O-O Bond Cleavage, and Reactivity. *J. Am. Chem. Soc.* **2019**, *141*, 15046−15057. (f) Coggins, M. K.; Sun, X.; Kwak, Y.; Solomon, E. I.; Rybak-Akimova, E.; Kovacs, J. A. Characterization of Metastable Intermediates Formed in the Reaction between a Mn(II) Complex and Dioxygen, Including a Crystallographic Structure of a Binuclear Mn(III)-Peroxo Species. *J. Am. Chem. Soc.* **2013**, *135*, 5631−5640. (g) Shook, R. L.; Peterson, S. M.; Greaves, J.; Moore, C.; Rheingold, A. L.; Borovik, A. S. Catalytic Reduction of Dioxygen to Water with a Monomeric Manganese Complex at Room Temperature. *J. Am. Chem. Soc.* **2011**, *133*, 5810−5817. (h) Geiger, R. A.; Chattopadhyay, S.; Day, V. W.; Jackson, T. A. A Series of Peroxomanganese(III) Complexes Supported by Tetradentate Aminopyridyl Ligands: Detailed Spectroscopic and Computational Studies. *J. Am. Chem. Soc.* **2010**, *132*, 2821−2831. (i) Shook, R. L.; Gunderson, W. A.; Greaves, J.; Ziller, J. W.; Hendrich, M. P.; Borovik, A. S. A Monomeric MnIII−Peroxo Complex Derived Directly from Dioxygen. *J. Am. Chem. Soc.* **2008**, *130*, 8888−8889. (j) Seo, M. S.; Kim, J. Y.; Annaraj, J.; Kim, Y.; Lee, Y.-M.; Kim, S.-J.; Kim, J.; Nam, W. [Mn(tmc)-(O2)]+: A Side-On Peroxido Manganese(III) Complex Bearing a Non-Heme Ligand. *Angew. Chem., Int. Ed.* **2007**, *46*, 377−380.

(11) **Group VIII:** (a) Costas, M.; Mehn, M. P.; Jensen, M. P.; Que, L., Jr. Dioxygen Activation at Mononuclear Nonheme Iron Active Sites: Enzymes, Models, and Intermediates. *Chem. Rev.* **2004**, *104*, 939−986. (b) Walleck, S.; Zimmermann, T. P.; Hachmeister, H.; Pilger, C.; Huser, T.; Katz, S.; Hildebrandt, P.; Stammler, A.; Bögge, H.; Bill, E.; Glaser, T. Generation of a μ-1,2-hydroperoxo FeIIIFeIII and a μ-1,2-peroxo FeIVFeIII Complex. *Nat. Commun.* **2022**, *13*, 1376. (c) Casadevall, C.; Martin-Diaconescu, V.; Browne, W. R.; Fernández, S.; Franco, F.; Cabello, N.; Benet-Buchholz, J.; Lassalle-Kaiser, B.; Lloret-Fillol, J. Isolation of a Ru(iv) side-on peroxo intermediate in the water oxidation reaction. *Nat. Chem.* **2021**, *13*, 800−804. (d) Banerjee, S.; Draksharapu, A.; Crossland, P. M.; Fan, R.; Guo, Y.; Swart, M.; Que, L. Sc3+-Promoted O-O Bond Cleavage of a (μ-1,2-Peroxo)diiron(III) Species Formed from an Iron(II) Precursor and O2 to Generate a Complex with an FeIV2(μ-O)2 Core. *J. Am. Chem. Soc.* **2020**, *142*, 4285−4297. (e) Jasniewski, A. J.; Komor, A. J.; Lipscomb, J. D.; Que, L., Jr. Unprecedented (μ-1,1-Peroxo)diferric Structure for the Ambiphilic Orange Peroxo Intermediate of the Nonheme N-Oxygenase CmlI. *J. Am. Chem. Soc.* **2017**, *139*, 10472−10485. (f) Cho, J.; Jeon, S.; Wilson, S. A.; Liu, L. V.; Kang, E. A.; Braymer, J. J.; Lim, M. H.; Hedman, B.; Hodgson, K. O.; Valentine, J. S.; Solomon, E. I.; Nam, W. Structure and reactivity of a mononuclear non-haem iron(III)-peroxo complex. *Nature* **2011**, *478*, 502−505. (g) Roelfes, G.; Vrajmasu, V.; Chen, K.; Ho, R. Y. N.; Rohde, J.-U.; Zondervan, C.; la Crois, R. M.; Schudde, E. P.; Lutz, M.; Spek, A. L.; Hage, R.; Feringa, B. L.; Münck, E.; Que, L. End-On and Side-On Peroxo Derivatives of Non-Heme Iron Complexes with Pentadentate Ligands: Models for Putative Intermediates in Biological Iron/Dioxygen Chemistry. *Inorg. Chem.* **2003**, *42*, 2639−2653. (h) Dong, Y.; Yan, S.; Young, V. G., Jr; Que, L., Jr Crystal Structure Analysis of a Synthetic Non-Heme Diiron O2 Adduct: Insight into the Mechanism of Oxygen Activation. *Angew. Chem., Int. Ed.* **1996**, *35*, 618−620.

(12) **Group IX:** (a) Wang, H.-Y.; Mijangos, E.; Ott, S.; Thapper, A. Water Oxidation Catalyzed by a Dinuclear Cobalt-Polypyridine Complex. *Angew. Chem., Int. Ed.* **2014**, *53*, 14499−14502. (b) Fukuzumi, S.; Mandal, S.; Mase, K.; Ohkubo, K.; Park, H.; Benet-Buchholz, J.; Nam, W.; Llobet, A. Catalytic Four-Electron Reduction of O2 via Rate-Determining Proton-Coupled Electron Transfer to a Dinuclear Cobalt-μ-1,2-peroxo Complex. *J. Am. Chem. Soc.* **2012**, *134*, 9906−9909. (c) Cho, J.; Sarangi, R.; Kang, H. Y.; Lee, J. Y.; Kubo, M.; Ogura, T.; Solomon, E. I.; Nam, W. Synthesis, Structural, and Spectroscopic Characterization and Reactivities of Mononuclear Cobalt(III)−Peroxo Complexes. *J. Am. Chem. Soc.* **2010**, *132*, 16977−16986. (d) Mimoun, H.; Perez Machirant, M. M.; Seree de Roch, I. Activation of molecular oxygen: rhodium-catalyzed oxidation of olefins. *J. Am. Chem. Soc.* **1978**, *100*, 5437−5444.

(13) **Group X:** (a) Boisvert, L.; Goldberg, K. I. Reactions of Late Transition Metal Complexes with Molecular Oxygen. *Acc. Chem. Res.* **2012**, *45*, 899−910. (b) Zhou, M.; Crabtree, R. H.; C−, H. C-H oxidation by platinum group metal oxo or peroxo species. *Chem. Soc. Rev.* **2011**, *40*, 1875−1884. (c) Kieber-Emmons, M. T.; Riordan, C. G. Dioxygen Activation at Monovalent Nickel. *Acc. Chem. Res.* **2007**, *40*, 618−625. (d) Zhao, N.; Filatov, A. S.; Xie, J.; Hill, E. A.; Rogachev, A. Y.; Anderson, J. S. Generation and Reactivity of a NiIII2(μ-1,2-peroxo) Complex. *J. Am. Chem. Soc.* **2020**, *142*, 21634−21639. (e) Duan, P.-C.; Manz, D.-H.; Dechert, S.; Demeshko, S.; Meyer, F. Reductive O2 Binding at a Dihydride Complex Leading to Redox Interconvertible μ-1,2-Peroxo and μ-1,2-Superoxo Dinickel(II) Intermediates. *J. Am. Chem. Soc.* **2018**, *140*, 4929−4939. (f) Yao, S.; Xiong, Y.; Vogt, M.; Grützmacher, H.; Herwig, C.; Limberg, C.; Driess, M. O−O Bond Activation in Heterobimetallic Peroxides: Synthesis of the Peroxide [LNi(μ,η2:η2-O2)K] and its Conversion into a Bis(μ-Hydroxo) Nickel Zinc Complex. *Angew. Chem., Int. Ed.* **2009**, *48*, 8107−8110. (g) Cho, J.; Sarangi, R.; Annaraj, J.; Kim, S. Y.; Kubo, M.; Ogura, T.; Solomon, E. I.; Nam, W. Geometric and electronic structure and reactivity of a mononuclear 'side-on' nickel(iii)-peroxo complex. *Nat. Chem.* **2009**, *1*, 568−572. (h) Stahl, S. S.; Thorman, J. L.; Nelson, R. C.; Kozee, M. A. Oxygenation of Nitrogen-Coordinated Palladium(0): Synthetic, Structural, and Mechanistic Studies and Implications for Aerobic Oxidation Catalysis. *J. Am. Chem. Soc.* **2001**, *123*, 7188−7189. (i) Wilke, G.; Schott, H.; Heimbach, P. Oxygen Complexes of Zerovalent Nickel, Palladium, and Platinum. *Angew. Chem., Int. Ed.* **1967**, *6*, 92−93.

(14) **Group XI:** (a) Elwell, C. E.; Gagnon, N. L.; Neisen, B. D.; Dhar, D.; Spaeth, A. D.; Yee, G. M.; Tolman, W. B. Copper-Oxygen Complexes Revisited: Structures, Spectroscopy, and Reactivity. *Chem. Rev.* **2017**, *117*, 2059−2107. (b) Brinkmeier, A.; Dalle, K. E.;

https://doi.org/10.1021/jacs.2c08140
J. Am. Chem. Soc. 2022, 144, 17295−17306

D'Amore, L.; Schulz, R. A.; Dechert, S.; Demeshko, S.; Swart, M.; Meyer, F. Modulation of a μ-1,2-Peroxo Dicopper(II) Intermediate by Strong Interaction with Alkali Metal Ions. *J. Am. Chem. Soc.* **2021**, *143*, 17751−17760. (c) Vargo, N. P.; Harland, J. B.; Musselman, B. W.; Lehnert, N.; Ertem, M. Z.; Robinson, J. R. Calcium-Ion Binding Mediates the Reversible Interconversion of Cis and Trans Peroxido Dicopper Cores. *Angew. Chem., Int. Ed.* **2021**, *60*, 19836−19842. (d) Dalle, K. E.; Gruene, T.; Dechert, S.; Demeshko, S.; Meyer, F. Weakly Coupled Biologically Relevant CuII2(μ-η1:η1-O2) cis-Peroxo Adduct that Binds Side-On to Additional Metal Ions. *J. Am. Chem. Soc.* **2014**, *136*, 7428−7434. (e) Kitajima, N.; Fujisawa, K.; Fujimoto, C.; Morooka, Y.; Hashimoto, S.; Kitagawa, T.; Toriumi, K.; Tatsumi, K.; Nakamura, A. A new model for dioxygen binding in hemocyanin. Synthesis, characterization, and molecular structure of the .mu.-.eta.2:.eta.2 peroxo dinuclear copper(II) complexes, [Cu(HB(3,5-R2pz)3)]2(O2) (R = isopropyl and Ph). *J. Am. Chem. Soc.* **1992**, *114*, 1277−1291. (f) Kitajima, N.; Fujisawa, K.; Morooka, Y.; Toriumi, K. .mu.-.eta.2:.eta.2-Peroxo binuclear copper complex, [Cu(HB(3,5-(Me2CH)2pz)3)]2(O2). *J. Am. Chem. Soc.* **1989**, *111*, 8975−8976. (g) Jacobson, R. R.; Tyeklar, Z.; Farooq, A.; Karlin, K. D.; Liu, S.; Zubieta, J. A copper-oxygen (Cu2-O2) complex. Crystal structure and characterization of a reversible dioxygen binding system. *J. Am. Chem. Soc.* **1988**, *110*, 3690−3692.

(15) (a) Deubel, D. V. Thianthrene 5-Oxide as a Probe for the Electronic Character of Oxygen-Transfer Reactions: Re-interpretation of Experiments Required,. *J. Org. Chem.* **2001**, *66*, 2686−2691. (b) Sisemore, M. F.; Selke, M.; Burstyn, J. N.; Valentine, J. S. Metalloporphyrin Peroxo Complexes of Iron(III), Manganese(III), and Titanium(IV). Comparative Studies Demonstrating That the Iron(III) Complex Is Extremely Nucleophilic. *Inorg. Chem.* **1997**, *36*, 979−984. (c) Ballistreri, F. P.; Tomaselli, G. A.; Toscano, R. M.; Conte, V.; Di Furia, F. Application of the thianthrene 5-oxide mechanistic probe to peroxometal complexes. *J. Am. Chem. Soc.* **1991**, *113*, 6209−6212. (d) Mimoun, H. Oxygen Transfer from Inorganic and Organic Peroxides to Organic Substrates: A Common Mechanism? *Angew. Chem., Int. Ed.* **1982**, *21*, 734−750. (e) Di Furia, F.; Modena, G. Mechanism of oxygen transfer from peroxo species. *Pure Appl. Chem.* **1982**, *54*, 1853−1866.

(16) (a) Ray, K.; Pfaff, F. F.; Wang, B.; Nam, W. Status of Reactive Non-Heme Metal-Oxygen Intermediates in Chemical and Enzymatic Reactions. *J. Am. Chem. Soc.* **2014**, *136*, 13942−13958. (b) Yudanov, I. V. Mechanism of olefin epoxidation with transition metal peroxo complexes: DFT study. *J. Struct. Chem.* **2007**, *48*, S111−S124. (c) Mimoun, H. The role of peroxymetallation in selective oxidative processes. *J. Mol. Catal.* **1980**, *7*, 1−29. (d) Regen, S. L.; Whitesides, G. M. Reactions of transition metal peroxides with n-butyllithium. *J. Organomet. Chem.* **1973**, *59*, 293−297. (e) Kholdeeva, O. A.; Trubitsina, T. A.; Maksimovskaya, R. I.; Golovin, A. V.; Neiwert, W. A.; Kolesov, B. A.; López, X.; Poblet, J. M. First Isolated Active Titanium Peroxo Complex: Characterization and Theoretical Study. *Inorg. Chem.* **2004**, *43*, 2284−2292. (f) Mimoun, H.; Postel, M.; Casabianca, F.; Fischer, J.; Mitschler, A. Novel unusually stable peroxotitanium(IV) compounds. Molecular and crystal structure of peroxobis(picolinato)(hexamethylphosphoric triamide)titanium(IV). *Inorg. Chem.* **1982**, *21*, 1303−1306. (g) Maksimchuk, N. V.; Ivanchikova, I. D.; Maksimov, G. M.; Eltsov, I. V.; Evtushok, V. Y.; Kholdeeva, O. A.; Lebbie, D.; Errington, R. J.; Solé-Daura, A.; Poblet, J. M.; Carbó, J. J. Why Does Nb(V) Show Higher Heterolytic Pathway Selectivity Than Ti(IV) in Epoxidation with H2O2? Answers from Model Studies on Nb- and Ti-Substituted Lindqvist Tungstates. *ACS Catal.* **2019**, *9*, 6262−6275. (h) Conte, V.; Coletti, A.; Floris, B.; Licini, G.; Zonta, C. Mechanistic aspects of vanadium catalysed oxidations with peroxides. *Coord. Chem. Rev.* **2011**, *255*, 2165−2177. (i) Mimoun, H.; Saussine, L.; Daire, E.; Postel, M.; Fischer, J.; Weiss, R. Vanadium(V) peroxy complexes. New versatile biomimetic reagents for epoxidation of olefins and hydroxylation of alkanes and aromatic hydrocarbons. *J. Am. Chem. Soc.* **1983**, *105*, 3101−3110. (j) Ballistreri, F. P.; Barbuzzi, E. G. M.; Tomaselli, G. A.; Toscano, R. M. Multiplicity of Reaction Pathways in the Processes of Oxygen Transfer to Secondary Amines by Mo(VI) and W(VI) Peroxo Complexes. *J. Org. Chem.* **1996**, *61*, 6381−6387. (k) Sharpless, K. B.; Townsend, J. M.; Williams, D. R. Mechanism of epoxidation of olefins by covalent peroxides of molybdenum(VI). *J. Am. Chem. Soc.* **1972**, *94*, 295−296. (l) Mimoun, H.; Seree de Roch, I.; Sajus, L. Epoxydation des olefines par les complexes peroxydiques covalents du molybdene-VI. *Tetrahedron* **1970**, *26*, 37−50. (m) Cantú Reinhard, F. G.; Barman, P.; Mukherjee, G.; Kumar, J.; Kumar, D.; Kumar, D.; Sastri, C. V.; de Visser, S. P. Keto-Enol Tautomerization Triggers an Electrophilic Aldehyde Deformylation Reaction by a Nonheme Manganese(III)-Peroxo Complex. *J. Am. Chem. Soc.* **2017**, *139*, 18328−18338. (n) Barman, P.; Upadhyay, P.; Faponle, A. S.; Kumar, J.; Nag, S. S.; Kumar, D.; Sastri, C. V.; de Visser, S. P. Deformylation Reaction by a Nonheme Manganese(III)-Peroxo Complex via Initial Hydrogen-Atom Abstraction. *Angew. Chem., Int. Ed.* **2016**, *55*, 11091−11095. (o) Zhu, W.; Jang, S.; Xiong, J.; Ezhov, R.; Li, X. X.; Kim, T.; Seo, M. S.; Lee, Y. M.; Pushkar, Y.; Sarangi, R.; Guo, Y.; Nam, W. A Mononuclear Non-heme Iron(III)-Peroxo Complex with an Unprecedented High O-O Stretch and Electrophilic Reactivity. *J. Am. Chem. Soc.* **2021**, *143*, 15556−15561. (p) Chandra, A.; Ansari, M.; Monte-Pérez, I.; Kundu, S.; Rajaraman, G.; Ray, K. Ligand-Constraint-Induced Peroxide Activation for Electrophilic Reactivity. *Angew. Chem., Int. Ed.* **2021**, *60*, 14954−14959. (q) Sen, A.; Halpern, J. Role of transition metal-dioxygen complexes in catalytic oxidation. Catalysis of the oxidation of phosphines by dioxygen adducts of platinum. *J. Am. Chem. Soc.* **1977**, *99*, 8337−8339. (r) Qayyum, M. F.; Sarangi, R.; Fujisawa, K.; Stack, T. D. P.; Karlin, K. D.; Hodgson, K. O.; Hedman, B.; Solomon, E. I. L-Edge X-ray Absorption Spectroscopy and DFT Calculations on Cu2O2 Species: Direct Electrophilic Aromatic Attack by Side-on Peroxo Bridged Dicopper(II) Complexes. *J. Am. Chem. Soc.* **2013**, *135*, 17417−17431. (s) Hoffmann, A.; Citek, C.; Binder, S.; Goos, A.; Rübhausen, M.; Troeppner, O.; Ivanović-Burmazović, I.; Wasinger, E. C.; Stack, T. D. P.; Herres-Pawlis, S. Catalytic Phenol Hydroxylation with Dioxygen: Extension of the Tyrosinase Mechanism beyond the Protein Matrix. *Angew. Chem., Int. Ed.* **2013**, *52*, 5398−5401. (t) Citek, C.; Lyons, C. T.; Wasinger, E. C.; Stack, T. D. P. Self-assembly of the oxy-tyrosinase core and the fundamental components of phenolic hydroxylation. *Nat. Chem.* **2012**, *4*, 317−322. (u) Itoh, S.; Kumei, H.; Taki, M.; Nagatomo, S.; Kitagawa, T.; Fukuzumi, S. Oxygenation of Phenols to Catechols by A (μ-η2:η2-Peroxo)-dicopper(II) Complex: Mechanistic Insight into the Phenolase Activity of Tyrosinase. *J. Am. Chem. Soc.* **2001**, *123*, 6708−6709. (v) Karlin, K. D.; Nasir, M. S.; Cohen, B. I.; Cruse, R. W.; Kaderli, S.; Zuberbuehler, A. D. Reversible Dioxygen Binding and Aromatic Hydroxylation in O2-Reactions with Substituted Xylyl Dinuclear Copper(I) Complexes: Syntheses and Low-Temperature Kinetic/Thermodynamic and Spectroscopic Investigations of a Copper Monooxygenase Model System. *J. Am. Chem. Soc.* **1994**, *116*, 1324−1336.

(17) (a) Kang, H.; Cho, J.; Cho, K.-B.; Nomura, T.; Ogura, T.; Nam, W. Mononuclear Manganese-Peroxo and Bis(μ-oxo)dimanganese Complexes Bearing a Common N-Methylated Macrocyclic Ligand. *Chem.—Eur. J.* **2013**, *19*, 14119−14125. (b) Annaraj, J.; Cho, J.; Lee, Y.-M.; Kim, S. Y.; Latifi, R.; de Visser, S. P.; Nam, W. Structural Characterization and Remarkable Axial Ligand Effect on the Nucleophilic Reactivity of a Nonheme Manganese(III)-Peroxo Complex. *Angew. Chem., Int. Ed.* **2009**, *48*, 4150−4153. (c) Shokri, A.; Que, L. Conversion of Aldehyde to Alkane by a Peroxoiron(III) Complex: A Functional Model for the Cyanobacterial Aldehyde-Deformylating Oxygenase. *J. Am. Chem. Soc.* **2015**, *137*, 7686−7691. (d) Park, M. J.; Lee, J.; Suh, Y.; Kim, J.; Nam, W. Reactivities of Mononuclear Non-Heme Iron Intermediates Including Evidence that Iron(III)−Hydroperoxo Species Is a Sluggish Oxidant. *J. Am. Chem. Soc.* **2006**, *128*, 2630−2634. (e) Wertz, D. L.; Valentine, J. S.Nucleophilicity of Iron-Peroxo Porphyrin Complexes. In *Metal-Oxo and Metal-Peroxo Species in Catalytic Oxidations*; Meunier, B., Ed.; Springer Berlin Heidelberg: Berlin, Heidelberg, 2000; pp 37−60. (f) Selke, M.; Valentine, J. S. Switching on the Nucleophilic Reactivity

https://doi.org/10.1021/jacs.2c08140
J. Am. Chem. Soc. 2022, 144, 17295−17306

of a Ferric Porphyrin Peroxo Complex. *J. Am. Chem. Soc.* **1998**, *120*, 2652−2653. (g) Selke, M.; Sisemore, M. F.; Valentine, J. S. The Diverse Reactivity of Peroxy Ferric Porphyrin Complexes of Electron-Rich and Electron-Poor Porphyrins. *J. Am. Chem. Soc.* **1996**, *118*, 2008−2012. (h) Sheldon, R. A.; Van Doorn, J. A. Cycloaddition of group VIII metal-dioxygen complexes to electrophilic olefins. *J. Organomet. Chem.* **1975**, *94*, 115−129. (i) Hu, X.; Castro-Rodriguez, I.; Meyer, K. Dioxygen Activation by a Low-Valent Cobalt Complex Employing a Flexible Tripodal N-Heterocyclic Carbene Ligand. *J. Am. Chem. Soc.* **2004**, *126*, 13464−13473.

(18) (a) Fukuzumi, S.; Cho, K. B.; Lee, Y. M.; Hong, S.; Nam, W. Mechanistic dichotomies in redox reactions of mononuclear metal-oxygen intermediates. *Chem. Soc. Rev.* **2020**, *49*, 8988−9027. (b) Sankaralingam, M.; Lee, Y.-M.; Nam, W.; Fukuzumi, S. Amphoteric reactivity of metal-oxygen complexes in oxidation reactions. *Coord. Chem. Rev.* **2018**, *365*, 41−59. (c) Bae, S. H.; Lee, Y. M.; Fukuzumi, S.; Nam, W. Fine Control of the Redox Reactivity of a Nonheme Iron(III)-Peroxo Complex by Binding Redox-Inactive Metal Ions. *Angew. Chem., Int. Ed.* **2017**, *56*, 801−805. (d) Cho, J.; Jeon, S.; Wilson, S. A.; Liu, L. V.; Kang, E. A.; Braymer, J. J.; Lim, M. H.; Hedman, B.; Hodgson, K. O.; Valentine, J. S.; Solomon, E. I.; Nam, W. Structure and reactivity of a mononuclear non-haem iron(III)-peroxo complex. *Nature* **2011**, *478*, 502−505.

(19) (a) Zhou, X.; Pang, Y.; Liu, Z.; Vovk, E. I.; van Bavel, A. P.; Li, S.; Yang, Y. Active oxygen center in oxidative coupling of methane on La2O3 catalyst. *J. Energy Chem.* **2021**, *60*, 649−659. (b) Liu, Z.; Ho Li, J. P.; Vovk, E.; Zhu, Y.; Li, S.; Wang, S.; van Bavel, A. P.; Yang, Y. Online Kinetics Study of Oxidative Coupling of Methane over La2O3 for Methane Activation: What Is Behind the Distinguished Light-off Temperatures? *ACS Catal.* **2018**, *8*, 11761−11772. (c) Jing, X. L.; Chen, Q. C.; He, C.; Zhu, X. Q.; Weng, W. Z.; Xia, W. S.; Wan, H. L. Mechanistic aspects of photo-induced formation of peroxide ions on the surface of cubic Ln2O3 (Ln = Nd, Sm, Gd) under oxygen. *Phys. Chem. Chem. Phys.* **2012**, *14*, 6898−6904. (d) Jing, X.; She, W.; Weng, W.; Li, J.; Xia, W.; Wan, H. 18O isotopic study of photo-induced formation of peroxide species on cubic Nd2O3. *Chin. J. Catal.* **2014**, *35*, 1385−1393. (e) Jing, X. L.; She, W. Y.; Li, J. M.; Chen, Q. C.; Weng, W. Z.; An, D. L.; Wan, H. L. Photoinduced Formation of Peroxide Ions on La2O3and Nd2O3under O2: Effects of Excitation Wavelength and Crystal Structure. *Chem.−Asian J.* **2015**, *10*, 2162−2168. (f) Weng, W. Z.; Wan, H. L.; Li, J. M.; Cao, Z. X. Laser-induced formation of metal-peroxide linkages on the surface of lanthanum sesquioxide under oxygen. *Angew. Chem., Int. Ed.* **2004**, *43*, 975−977. (g) Huang, P.; Zhao, Y.; Zhang, J.; Zhu, Y.; Sun, Y. Exploiting shape effects of La2O3 nanocatalysts for oxidative coupling of methane reaction. *Nanoscale* **2013**, *5*, 10844−10848. (h) Chu, C.; Zhao, Y.; Li, S.; Sun, Y. CO2 Chemisorption and Its Effect on Methane Activation in La2O3-Catalyzed Oxidative Coupling of Methane. *J. Phys. Chem. C* **2016**, *120*, 2737−2746. (i) Ma, Z.; Mahmudov, K. T.; Aliyeva, V. A.; Gurbanov, A. V.; Guedes da Silva, M. F. C.; Pombeiro, A. J. L. Peroxides in metal complex catalysis. *Coord. Chem. Rev.* **2021**, *437*, 213859. (j) Lei, Y.; Chu, C.; Li, S.; Sun, Y. Methane Activations by Lanthanum Oxide Clusters. *J. Phys. Chem. C* **2014**, *118*, 7932−7945. (k) Guzman, J.; Carrettin, S.; Fierro-Gonzalez, J. C.; Hao, Y.; Gates, B. C.; Corma, A. CO oxidation catalyzed by supported gold: cooperation between gold and nanocrystalline rare-earth supports forms reactive surface superoxide and peroxide species. *Angew. Chem., Int. Ed.* **2005**, *44*, 4778−4781. (l) Chu, C.; Zhao, Y.; Li, S.; Sun, Y. Role of Peroxides on La2O3 Catalysts in Oxidative Coupling of Methane. *J. Phys. Chem. C* **2014**, *118*, 27954−27960. (m) Siakavelas, G. I.; Charisiou, N. D.; AlKhoori, A.; Sebastian, V.; Hinder, S. J.; Baker, M. A.; Yentekakis, I. V.; Polychronopoulou, K.; Goula, M. A. Cerium oxide catalysts for oxidative coupling of methane reaction: Effect of lithium, samarium and lanthanum dopants. *J. Environ. Chem. Eng.* **2022**, *10*, 107259. (n) Knözinger, H. In situ Raman spectroscopy. A powerful tool for studies in selective catalytic oxidation. *Catal. Today* **1996**, *32*, 71−80. (o) Wang, S.; Li, S.; Dixon, D. A. Mechanism of selective and complete oxidation in La2O3-catalyzed oxidative coupling of methane. *Catal. Sci. Technol.* **2020**, *10*, 2602−2614.

(20) (a) Hara, K.; Park, S. Y.; Yamagiwa, N.; Matsunaga, S.; Shibasaki, M. Catalytic Asymmetric Epoxidation of α,β-Unsaturated Phosphane Oxides with a Y(O-iPr)3/Biphenyldiol Complex. *Chem.−Asian J.* **2008**, *3*, 1500−1504. (b) Kakei, H.; Tsuji, R.; Ohshima, T.; Morimoto, H.; Matsunaga, S.; Shibasaki, M. Catalytic Asymmetric Epoxidation of α,β-Unsaturated Esters with Chiral Yttrium-Biaryldiol Complexes. *Chem.−Asian J.* **2007**, *2*, 257−264.

(21) (a) Kamitani, J. S.; Sumaoka, J.; Asanuma, H.; Komiyama, M. Efficient RNA hydrolysis by lanthanide(III)-hydrogen peroxide combinations. Novel aggregates as the catalytic species 1. *J. Chem. Soc., Perkin Trans. 2* **1998**, 523−528. (b) Takasaki, B. K.; Chin, J. Synergistic effect between lanthanum(III) and hydrogen peroxide in phosphate diester cleavage. *J. Am. Chem. Soc.* **1993**, *115*, 9337−9338. (c) Takasaki, B. K.; Chin, J. La(III)-Hydrogen Peroxide Cooperativity in Phosphate Diester Cleavage: A Mechanistic Study. *J. Am. Chem. Soc.* **1995**, *117*, 8582−8585. (d) Takasaki, B. K.; Chin, J. Cleavage of the Phosphate Diester Backbone of DNA with Cerium(III) and Molecular Oxygen. *J. Am. Chem. Soc.* **1994**, *116*, 1121−1122.

(22) (a) Farnaby, J. H.; Fang, M.; Ziller, J. W.; Evans, W. J. Expanding yttrium bis(trimethylsilylamide) chemistry through the reaction chemistry of (N2)2-, (N2)3-, and (NO)2- complexes. *Inorg. Chem.* **2012**, *51*, 11168−11176. (b) Qasim, H. M.; Ayass, W. W.; Donfack, P.; Mougharbel, A. S.; Bhattacharya, S.; Nisar, T.; Balster, T.; Solé-Daura, A.; Römer, I.; Goura, J.; Materny, A.; Wagner, V.; Poblet, J. M.; Bassil, B. S.; Kortz, U. Peroxo-Cerium(IV)-Containing Polyoxometalates: [CeIV6(O2)9(GeW10O37)3]24-, a Recyclable Homogeneous Oxidation Catalyst. *Inorg. Chem.* **2019**, *58*, 11300−11307. (c) Paul, M.; Shirase, S.; Morimoto, Y.; Mathey, L.; Murugesapandian, B.; Tanaka, S.; Itoh, S.; Tsurugi, H.; Mashima, K. Cerium-Complex-Catalyzed Oxidation of Arylmethanols under Atmospheric Pressure of Dioxygen and Its Mechanism through a Side-On μ-Peroxo Dicerium(IV) Complex. *Chemistry* **2016**, *22*, 4008−4014.

(23) (a) Niemeyer, M. Synthesis and Structural Characterization of Several Ytterbium Bis(trimethylsilyl)amides Including Base-free [Yb{N(SiMe3)2}2(μ-Cl)]2 - A Coordinatively Unsaturated Complex with Additional Agostic Yb···(H3C-Si) Interactions. *Z. Anorg. Allg. Chem.* **2002**, *628*, 647−657. (b) Deacon, G. B.; Forsyth, C. M.; Freckmann, D.; Junk, P. C.; Konstas, K.; Luu, J.; Meyer, G.; Werner, D. Adventitiously Obtained Rare-Earth Peroxide Complexes and Their Structural Characterisation. *Aust. J. Chem.* **2014**, *67*, 1860−1865. (c) Xémard, M.; Goudy, V.; Braun, A.; Tricoire, M.; Cordier, M.; Ricard, L.; Castro, L.; Louyriac, E.; Kefalidis, C. E.; Clavaguéra, C.; Maron, L.; Nocton, G. Reductive Disproportionation of CO2 with Bulky Divalent Samarium Complexes. *Organometallics* **2017**, *36*, 4660−4668. (d) van Velzen, N. J. C.; Harder, S. Deca-Arylsamarocene: An Unusually Inert Sm(II) Sandwich Complex. *Organometallics* **2018**, *37*, 2263−2271. (e) Deng, D. L.; Zhang, Y.-H.; Dai, C.-Y.; Zeng, H.; Ye, C.-Q.; Hage, R. Lanthanide superoxide complexes and a novel μ3-oxo samarium complex with hydrotris(3,5-dimethylpyrazolyl)borate ligand. *Inorg. Chim. Acta* **2000**, *310*, 51−55.

(24) (a) Neumüller, B.; Weller, F.; Gröb, T.; Dehnicke, K. Lanthanoid-Peroxo-Komplexe mit μ3-η2:η2:η2-(O22)-Koordination. Die Kristallstrukturen von [Ln4(O2)2Cl8(Py)10] Py mit Ln Sm, Eu, Gd. *Z. Anorg. Allg. Chem.* **2002**, *628*, 2365−2371. (b) Roitershtein, D. M. V.; Vinogradov, A. A.; Lyssenko, K. A.; Nifant'ev, I. E. Self-assembly of heteroleptic tetranuclear carboxylate complexes of yttrium and lanthanides during hydrolysis and oxidation of rare earth homoleptic carboxylates. *Inorg. Chem. Commun.* **2017**, *84*, 225−228.

(25) (a) Gee, W. J.; MacLellan, J. G.; Forsyth, C. M.; Moubaraki, B.; Murray, K. S.; Andrews, P. C.; Junk, P. C. Caging peroxide: anion-templated synthesis and characterization of a rare-earth cluster. *Inorg. Chem.* **2012**, *51*, 8661−8663. (b) Patroniak, V.; Kubicki, M.; Mondry, A.; Lisowski, J.; Radecka-Paryzek, W. Pentaaza macrocyclic ytterbium-(iii) complex and solvent controlled supramolecular self-assembly of its dimeric μ-η2:η2peroxo-bridged derivatives. *Dalton Trans.* **2004**,

https://doi.org/10.1021/jacs.2c08140
J. Am. Chem. Soc. 2022, 144, 17295−17306

3295−3304. (c) Patroniak, V. K.; Kubicki, M.; Radecka-Paryzek, W. The First Example of μ-η2:η2-Peroxo-Bridged Macrocyclic Lanthanide Complex. The Crystal Structure of [Lu2{Me2pyo[16]trieneN5}-2(μ-η2:η2-O2)Cl2](ClO4)2Dioxane Solvate. *J. Inclusion Phenom. Macrocyclic Chem.* **2004**, *49*, 121−125. (d) Radecka-Paryzek, W.; Patroniak, V.; Kubicki, M. First example of template synthesis of pentaaza macrocyclic ytterbium(III) complex and solvent-controlled supramolecular self-assembly of its dimeric μ-η 2 :η 2 peroxo-bridged derivative. *Inorg. Chem. Commun.* **2004**, *7*, 455−458. (e) Gregoliński, J.; Ślepokura, K. Monomeric and dimeric nitrate lanthanide(III) and yttrium(III) coordination compounds of (2 + 2) imine macrocycle derived from 2,6-diformylpyridine and trans-1,2-diaminocyclopentane. *Polyhedron* **2020**, *181*, 114433. (f) Miller, J. T.; Ren, Y.; Li, S.; Tan, K.; McCandless, G.; Jacob, C.; Wu, Z.; Chu, C. W.; Lv, B.; Biewer, M. C.; Stefan, M. C. Peroxide-Templated Assembly of a Trimetal Neodymium Complex Single-Molecule Magnet. *Inorg. Chem.* **2020**, *59*, 10379−10383.

(26) Henthorn, J. T.; Agapie, T. Dioxygen reactivity with a ferrocene-Lewis acid pairing: reduction to a boron peroxide in the presence of tris(pentafluorophenyl)borane. *Angew. Chem., Int. Ed.* **2014**, *53*, 12893−12896.

(27) Sigmund, L. M.; Ehlert, C.; Enders, M.; Graf, J.; Gryn'ova, G.; Greb, L. Dioxygen Activation and Pyrrole α-Cleavage with Calix[4]-pyrrolato Aluminates: Enzyme Model by Structural Constraint. *Angew. Chem., Int. Ed.* **2021**, *60*, 15632−15640.

(28) Dahl, E. W.; Kiernicki, J. J.; Zeller, M.; Szymczak, N. K. Hydrogen Bonds Dictate O2 Capture and Release within a Zinc Tripod. *J. Am. Chem. Soc.* **2018**, *140*, 10075−10079.

(29) Kakuda, S.; Rolle, C. J.; Ohkubo, K.; Siegler, M. A.; Karlin, K. D.; Fukuzumi, S. Lewis acid-induced change from four- to two-electron reduction of dioxygen catalyzed by copper complexes using scandium triflate. *J. Am. Chem. Soc.* **2015**, *137*, 3330−3337.

(30) (a) Fukuzumi, S.; Ohkubo, K.; Morimoto, Y. Mechanisms of metal ion-coupled electron transfer. *Phys. Chem. Chem. Phys.* **2012**, *14*, 8472−8484. (b) Fukuzumi, S.; Ohkubo, K.; Lee, Y. M.; Nam, W. Lewis Acid Coupled Electron Transfer of Metal-Oxygen Intermediates. *Chemistry* **2015**, *21*, 17548−17559. (c) Devi, T.; Lee, Y.-M.; Nam, W.; Fukuzumi, S. Metal ion-coupled electron-transfer reactions of metal-oxygen complexes. *Coord. Chem. Rev.* **2020**, *410*, 213219.

(31) (a) Fukuzumi, S.; Ohkubo, K. Quantitative Evaluation of Lewis Acidity of Metal Ions Derived from theg Values of ESR Spectra of Superoxide: Metal Ion Complexes in Relation to the Promoting Effects in Electron Transfer Reactions. *Chem.—Eur. J.* **2000**, *6*, 4532−4535. (b) Ohkubo, K.; Menon, S. C.; Orita, A.; Otera, J.; Fukuzumi, S. Quantitative Evaluation of Lewis Acidity of Metal Ions with Different Ligands and Counterions in Relation to the Promoting Effects of Lewis Acids on Electron Transfer Reduction of Oxygen. *J. Org. Chem.* **2003**, *68*, 4720−4726.

(32) MacDonald, M. R.; Bates, J. E.; Ziller, J. W.; Furche, F.; Evans, W. J. Completing the series of +2 ions for the lanthanide elements: synthesis of molecular complexes of Pr2+, Gd2+, Tb2+, and Lu2+. *J. Am. Chem. Soc.* **2013**, *135*, 9857−9868.

(33) (a) Noviandri, I.; Brown, K. N.; Fleming, D. S.; Gulyas, P. T.; Lay, P. A.; Masters, A. F.; Phillips, L. The Decamethylferrocenium/Decamethylferrocene Redox Couple: A Superior Redox Standard to the Ferrocenium/Ferrocene Redox Couple for Studying Solvent Effects on the Thermodynamics of Electron Transfer. *J. Phys. Chem. B* **1999**, *103*, 6713−6722. (b) Bard, A. J.; Faulkner, L. R.. *Electrochemical Methods: Fundamental and Applications*, 2nd ed.; John Wiley & Sons: Hoboken, NJ, 2001. p 3.

(34) (a) Johnston, D. H.; Shriver, D. F. Vibrational study of the trifluoromethanesulfonate anion: unambiguous assignment of the asymmetric stretching modes. *Inorg. Chem.* **2002**, *32*, 1045−1047. (b) Paul, P.; Ghosh, M.; Neogy, D.; Mallick, P. K. Electronic and vibrational spectra of some rare earth trifluoromethanesulfonates crystals. *Spectrochim. Acta, Part A* **2011**, *78*, 59−63.

(35) Shirase, S.; Shinohara, K.; Tsurugi, H.; Mashima, K. Oxidation of Alcohols to Carbonyl Compounds Catalyzed by Oxo-Bridged Dinuclear Cerium Complexes with Pentadentate Schiff-Base Ligands under a Dioxygen Atmosphere. *ACS Catal.* **2018**, *8*, 6939−6947.

(36) Mizuno, N.; Yamaguchi, K.; Kamata, K. Epoxidation of olefins with hydrogen peroxide catalyzed by polyoxometalates. *Coord. Chem. Rev.* **2005**, *249*, 1944−1956.

(37) Bagha, U. K.; Satpathy, J. K.; Mukherjee, G.; Sastri, C. V.; de Visser, S. P. A comprehensive insight into aldehyde deformylation: mechanistic implications from biology and chemistry. *Org. Biomol. Chem.* **2021**, *19*, 1879−1899.

(38) Barman, P.; Cantú Reinhard, F. G.; Bagha, U. K.; Kumar, D.; Sastri, C. V.; de Visser, S. P. Hydrogen by Deuterium Substitution in an Aldehyde Tunes the Regioselectivity by a Nonheme Manganese-(III)-Peroxo Complex. *Angew. Chem., Int. Ed.* **2019**, *58*, 10639−10643.

(39) (a) Gamba, I.; Palavicini, S.; Monzani, E.; Casella, L. Catalytic sulfoxidation by dinuclear copper complexes. *Chemistry* **2009**, *15*, 12932−12936. (b) So, H.; Park, Y. J.; Cho, K. B.; Lee, Y. M.; Seo, M. S.; Cho, J.; Sarangi, R.; Nam, W. Spectroscopic characterization and reactivity studies of a mononuclear nonheme Mn(III)-hydroperoxo complex. *J. Am. Chem. Soc.* **2014**, *136*, 12229−12232. (c) Kim, Y. M.; Cho, K. B.; Cho, J.; Wang, B.; Li, C.; Shaik, S.; Nam, W. A mononuclear non-heme high-spin iron(III)-hydroperoxo complex as an active oxidant in sulfoxidation reactions. *J. Am. Chem. Soc.* **2013**, *135*, 8838−8841.

(40) (a) Würtele, C.; Sander, O.; Lutz, V.; Waitz, T.; Tuczek, F.; Schindler, S. Aliphatic C-H Bond Oxidation of Toluene Using Copper Peroxo Complexes That Are Stable at Room Temperature. *J. Am. Chem. Soc.* **2009**, *131*, 7544−7545. (b) Rolff, M.; Schottenheim, J.; Decker, H.; Tuczek, F. Copper-O2 reactivity of tyrosinase models towards external monophenolic substrates: molecular mechanism and comparison with the enzyme. *Chem. Soc. Rev.* **2011**, *40*, 4077−4098.

(41) Rived, F.; Rosés, M.; Bosch, E. Dissociation constants of neutral and charged acids in methyl alcohol. The acid strength resolution. *Anal. Chim. Acta* **1998**, *374*, 309−324.

(42) (a) Saouma, C. T.; Kaminsky, W.; Mayer, J. M. Protonation and concerted proton-electron transfer reactivity of a bis-benzimidazolate ligated [2Fe-2S] model for Rieske clusters. *J. Am. Chem. Soc.* **2012**, *134*, 7293−7296. (b) McCarthy, B. D.; Martin, D. J.; Rountree, E. S.; Ullman, A. C.; Dempsey, J. L. Electrochemical Reduction of Brønsted Acids by Glassy Carbon in Acetonitrile-Implications for Electrocatalytic Hydrogen Evolution. *Inorg. Chem.* **2014**, *53*, 8350−8361.

(43) (a) Fomin, V. M.; Shirokov, A. E.; Polyakova, N. G. Features of the oxidation of certain hydroxy derivatives of ferrocene with molecular oxygen in organic solvents. *Russ. J. Gen. Chem.* **2008**, *78*, 1361−1370. (b) Fomin, V. M.; Markin, A. V. Oxidation mechanism of ferrocene with molecular oxygen. *J. Therm. Anal. Calorim.* **2008**, *92*, 985−987. (c) Fomin, V. M.; Shirokov, A. E.; Polyakova, N. G.; Smirnov, P. A. On the radical chain mechanism of oxidation of a series of ferrocene derivatives with molecular oxygen. *Russ. J. Gen. Chem.* **2007**, *77*, 652−653.

(44) (a) Fomin, V. M.; Shirokov, A. E. Mechanism of initiation of the radical chain oxidation by molecular oxygen of hydroxymethylferrocene and its ethyl ether in organic solvents. *Russ. J. Gen. Chem.* **2009**, *79*, 928−939. (b) Fomin, V. M.; Klimova, M. N.; Smirnov, A. S. Autooxidation of Ferrocenylacetic Acid in Organic Solvents. *Russ. J. Coord. Chem.* **2004**, *30*, 332−334.

(45) (a) Dong, X.; Robinson, J. R. The versatile roles of neutral donor ligands in tuning catalyst performance for the ring-opening polymerization of cyclic esters. *New J. Chem.* **2022**, *46*, 444−453. (b) Maity, S.; Flowers, R. A. Mechanistic Study and Development of Catalytic Reactions of Sm(II). *J. Am. Chem. Soc.* **2019**, *141*, 3207−3216. (c) Chciuk, T. V.; Anderson, W. R.; Flowers, R. A. Interplay between Substrate and Proton Donor Coordination in Reductions of Carbonyls by SmI2-Water Through Proton-Coupled Electron-Transfer. *J. Am. Chem. Soc.* **2018**, *140*, 15342−15352. (d) Chciuk, T. V.; Hilmersson, G.; Flowers, R. A. Solvent-Dependent Substrate Reduction by {Sm[N(SiMe3)2]2(THF)2}. An Alternative Approach for Accelerating the Rate of Substrate Reduction by Sm(II). *J. Org.*

https://doi.org/10.1021/jacs.2c08140
J. Am. Chem. Soc. 2022, 144, 17295−17306

Chem. **2014**, *79*, 9441−9443. (e) Hatano, M.; Ishihara, K. Lanthanum(iii) catalysts for highly efficient and chemoselective transesterification. *Chem. Commun.* **2013**, *49*, 1983−1997. (f) Sadasivam, D. V.; Teprovich, J. A.; Procter, D. J.; Flowers, R. A. Dynamic Ligand Exchange in Reactions of Samarium Diiodide. *Org. Lett.* **2010**, *12*, 4140−4143. (g) Sánchez-Lombardo, I.; Yatsimirsky, A. K. Simplified Speciation and Improved Phosphodiesterolytic Activity of Hydroxo Complexes of Trivalent Lanthanides in Aqueous DMSO. *Inorg. Chem.* **2008**, *47*, 2514−2525. (h) Sadasivam, D. V.; Antharjanam, P. K. S.; Prasad, E.; Flowers, R. A. Mechanistic Study of Samarium Diiodide-HMPA Initiated 5-exo-trig Ketyl−Olefin Coupling: The Role of HMPA in Post-Electron Transfer Steps. *J. Am. Chem. Soc.* **2008**, *130*, 7228−7229. (i) Prasad, E.; Knettle, B. W.; Flowers, R. A. The Role of Ligand Displacement in Sm(II)−HMPA-Based Reductions. *J. Am. Chem. Soc.* **2004**, *126*, 6891−6894.

(46) (a) Kobayashi, S.; Sugiura, M.; Kitagawa, H.; Lam, W. W. L. Rare-Earth Metal Triflates in Organic Synthesis. *Chem. Rev.* **2002**, *102*, 2227−2302. (b) Dissanayake, P.; Allen, M. J. Dynamic Measurements of Aqueous Lanthanide Triflate-Catalyzed Reactions Using Luminescence Decay. *J. Am. Chem. Soc.* **2009**, *131*, 6342−6343. (c) Tsang, J. S. W.; Neverov, A. A.; Brown, R. S. La3+-Catalyzed Methanolysis of Hydroxypropyl-p-nitrophenyl Phosphate as a Model for the RNA Transesterification Reaction. *J. Am. Chem. Soc.* **2003**, *125*, 1559−1566. (d) Tsang, J. S. W.; Neverov, A. A.; Brown, R. S. Billion-fold Acceleration of the Methanolysis of Paraoxon Promoted by La(OTf)3 in Methanol. *J. Am. Chem. Soc.* **2003**, *125*, 7602−7607. (e) Neverov, A. A.; Brown, R. S. La3+-Catalyzed Methanolysis of Phosphate Diesters. Remarkable Rate Acceleration of the Methanolysis of Diphenyl Phosphate, Methyl p-Nitrophenyl Phosphate, and Bis(p-nitrophenyl) Phosphate. *Inorg. Chem.* **2001**, *40*, 3588−3595.

(47) (a) Geary, W. J. THE USE OF CONDUCTIVITY MEASUREMENTS IN ORGANIC SOLVENTS FOR THE CHARACTERISATION OF COORDINATION COMPOUNDS. *Coord. Chem. Rev.* **1971**, *7*, 81−122. (b) van Loon, A. M.; van Bekkum, H.; Peters, J. A. Structures of Dysprosium(III) Triflates in Water, Methanol, and 2-Propanol As Studied by 17O and 19F NMR Spectroscopy. *Inorg. Chem.* **1999**, *38*, 3080−3084.

(48) Bünzli, J.-C. G.; Merbach, A. E.; Nielson, R. M. 139La NMR and Quantitative FT-IR Investigation of the Interaction between Ln(III) Ions and Various Anions in Organic Solvents. *Inorg. Chim. Acta* **1987**, *139*, 151−152.

(49) Hoops, S.; Sahle, S.; Gauges, R.; Lee, C.; Pahle, J.; Simus, N.; Singhal, M.; Xu, L.; Mendes, P.; Kummer, U. COPASI–a COmplex PAthway SImulator. *Bioinformatics* **2006**, *22*, 3067−3074.

(50) Zhao, Y.; Truhlar, D. G. A new local density functional for main-group thermochemistry, transition metal bonding, thermochemical kinetics, and noncovalent interactions. *J. Chem. Phys.* **2006**, *125*, 194101.

(51) Marenich, A. V.; Cramer, C. J.; Truhlar, D. G. Universal Solvation Model Based on Solute Electron Density and on a Continuum Model of the Solvent Defined by the Bulk Dielectric Constant and Atomic Surface Tensions. *J. Phys. Chem. B* **2009**, *113*, 6378−6396.

(52) (a) Laing, M. Gadolinium: Central Metal of the Lanthanoids. *J. Chem. Educ.* **2009**, *86*, 188−189. (b) Di Bernardo, P.; Melchior, A.; Tolazzi, M.; Zanonato, P. L. Thermodynamics of lanthanide(III) complexation in non-aqueous solvents. *Coord. Chem. Rev.* **2012**, *256*, 328−351.

(53) (a) Mioduski, T. The "Regular" and "Inverse" Tetrad Effect. *Comments Inorg. Chem.* **2006**, *19*, 93−119. (b) Persson, I.; D'Angelo, P.; De Panfilis, S.; Sandström, M.; Eriksson, L. Hydration of Lanthanoid(III) Ions in Aqueous Solution and Crystalline Hydrates Studied by EXAFS Spectroscopy and Crystallography: The Myth of the ″Gadolinium Break″. *Chemistry* **2008**, *14*, 3056−3066. (c) Peppard, D. F. M.; Mason, G. W.; Lewey, S. A tetrad effect in the liquid-liquid extraction ordering of lanthanides(III). *J. Inorg. Nucl. Chem.* **1969**, *31*, 2271−2272.

(54) (a) Hu, A.; Aluicio-Sarduy, E.; Brown, V.; MacMillan, S. N.; Becker, K. V.; Barnhart, T. E.; Radchenko, V.; Ramogida, C. F.; Engle, J. W.; Wilson, J. J. Py-Macrodipa: A Janus Chelator Capable of Binding Medicinally Relevant Rare-Earth Radiometals of Disparate Sizes. *J. Am. Chem. Soc.* **2021**, *143*, 10429−10440. (b) Hu, A.; MacMillan, S. N.; Wilson, J. J. Macrocyclic Ligands with an Unprecedented Size-Selectivity Pattern for the Lanthanide Ions. *J. Am. Chem. Soc.* **2020**, *142*, 13500−13506. (c) Deblonde, G. J. P.; Mattocks, J. A.; Park, D. M.; Reed, D. W.; Cotruvo, J. A.; Jiao, Y. Selective and Efficient Biomacromolecular Extraction of Rare-Earth Elements using Lanmodulin. *Inorg. Chem.* **2020**, *59*, 11855−11867. (d) Nash, K. L.; Brigham, D.; Shehee, T. C.; Martin, A. The kinetics of lanthanide complexation by EDTA and DTPA in lactate media. *Dalton Trans.* **2012**, *41*, 14547−14556. (e) Rojas-Quijano, F. A.; BenyÃ^3, E. T.; TircsÃ^3, G.; KÃilmÃin, F. K.; Baranyai, Z.; Aime, S.; Sherry, A. D.; KovÃics, Z. Lanthanide(III) Complexes of Tris(amide) PCTA Derivatives as Potential Bimodal Magnetic Resonance and Optical Imaging Agents. *Chem.—Eur. J.* **2009**, *15*, 13188−13200. (f) Miguirditchian, M.; Guillaneux, D.; Guillaumont, D.; Moisy, P.; Madic, C.; Jensen, M. P.; Nash, K. L. Thermodynamic Study of the Complexation of Trivalent Actinide and Lanthanide Cations by ADPTZ, a Tridentate N-Donor Ligand. *Inorg. Chem.* **2005**, *44*, 1404−1412.

(55) (a) Ramírez-Solís, A.; Bartulovich, C. O.; León-Pimentel, C. I.; Saint-Martin, H.; Boekell, N. G.; Flowers, R. A. Proton donor effects on the reactivity of SmI2. Experimental and theoretical studies on methanol solvation vs. aqueous solvation. *Dalton Trans.* **2020**, *49*, 7897−7902. (b) Ramirez-Solis, A.; Amaro-Estrada, J. I.; Hernández-Cobos, J.; Maron, L. Aqueous Solvation of SmI3: A Born-Oppenheimer Molecular Dynamics Density Functional Theory Cluster Approach. *Inorg. Chem.* **2018**, *57*, 2843−2850. (c) Ramírez-Solís, A.; Bartulovich, C. O.; Chciuk, T. V.; Hernández-Cobos, J.; Saint-Martin, H.; Maron, L.; Anderson, W. R., Jr.; Li, A. M.; Flowers, R. A. Experimental and Theoretical Studies on the Implications of Halide-Dependent Aqueous Solvation of Sm(II). *J. Am. Chem. Soc.* **2018**, *140*, 16731−16739.

https://doi.org/10.1021/jacs.2c08140
J. Am. Chem. Soc. 2022, 144, 17295−17306